Nonstandard string-SUSY scenario and its phenomenological implications

C.-H. Chen
Davis Institute for High Energy Physics, University of California, Davis, California 95616

M. Drees
Davis Institute for High Energy Physics, University of California, Davis, California 95616
and Physics Department, University of Wisconsin, Madison, Wisconsin 53706

J. F. Gunion
Davis Institute for High Energy Physics, University of California, Davis, California 95616
(Received 29 July 1996)

We investigate the phenomenology of an orbifold string model in which supersymmetry breaking is dominated by the overall ''size'' modulus field and all matter fields are in the untwisted sector. The possibly close degeneracy of the lightest neutralino and chargino and the possibly small splitting between the gluino and chargino or LSP mass imply that discovery of supersymmetry at future colliders could be more challenging than anticipated. Specialized search strategies and particular detector features could play an important role. For preferred model parameter choices, the phenomenology of dark matter in the universe is significantly modified. [S0556-2821(97)02601-5]

PACS number(s): 11.30.Pb, 12.10.−g, 12.60.Jv, 14.80.Ly

I. INTRODUCTION

In the conventional approach to supersymmetry breaking, a more or less standard set of boundary conditions at the grand unified theory (GUT) scale M_U has been most thoroughly studied. These are a universal gaugino mass $m_{1/2}$, a common scalar mass m_0, and a universal value for the soft A parameters. The effects of nondegeneracy among the scalar masses have recently been explored in many papers [1]. No systematic study of models with nonuniversal gaugino masses has appeared. In this paper, we explore one such model, motivated by the string theory picture, in which supersymmetry breaking is dominated by the overall ''size'' modulus field, as described in Ref. [2]. Models with multiple modulus fields are considered in Ref. [3]. In this latter paper, it is found that if tachyonic masses that could cause charge and color breaking are not allowed, then the soft supersymmetry- (SUSY) breaking boundary conditions cannot be such as to greatly distort results based on assuming that all the moduli fields participate in SUSY breaking equally, as is implicit when only the overall modulus field is employed. The boundary conditions that result when SUSY breaking is dominated by the overall size modulus field lead to an interesting and unusual SUSY phenomenology that differs substantially from that appropriate to universal boundary conditions in such diverse areas as cold dark matter in the Universe and direct SUSY search strategies or difficulties.

In the context of string model scenarios in which all the moduli fields participate equally through an overall modulus field, nonuniversality among the gaugino masses at M_U is not typical. This is because the only tree-level contributions to the gaugino masses are those originating from the dilaton field, and these are automatically universal. Nonuniversal contributions to the gaugino masses arise only at one loop. Thus, significant nonuniversality is only possible when SUSY breaking is not dominated by the dilaton, but rather by the overall modulus field. An additional motivation for considering a model with modulus (as opposed to dilaton) dominated SUSY breaking is the fact that essentially the whole of dilaton-dominated parameter space is excluded by the requirement that the standard SUSY vacuum should be deeper than the charge and color-breaking minima [4].

In the notation of Ref. [2], SUSY breaking becomes moduli dominated in the $\sin\theta\to 0$ limit, where θ is the goldstino angle and $\tan\theta$ measures the relative amount of SUSY breaking due to the dilaton field, S, relative to the overall size modulus field, T. In the $\sin\theta\to 0$ limit, the gaugino masses at M_U arise entirely from one-loop threshold and Kahler potential corrections. The masses are both small and typically very nonuniversal.

Although it is possible to take $\sin\theta\to 0$ in a general Calabi-Yau model, there is only one simple orbifold model in which $\sin\theta$ can be taken to be sufficiently near zero to avoid dilaton dominance and the resulting approximate universality of gaugino masses. This is the model (called the O-II scenario) in which all matter fields have modular weight $n=-1$, i.e., lie in the untwisted sector. (If any $n\neq -1$, then $\sin^2\theta \geq 1/2$ is required in order to avoid a negative mass squared for some squark or slepton.) The $\sin\theta\to 0$ limit of the O-II model is analogous to the effective large T limit of a Calabi-Yau model. We focus on the $\sin\theta\to 0$ limit of the O-II orbifold model since it is only for orbifold models that the required one-loop Kahler potential and threshold corrections have been computed. Although, this model is only one of many theories that yield nonuniversal gaugino masses, its phenomenology will provide a number of very valuable lessons and comparisons to the phenomenology typical of models with universal boundary conditions.

In the O-II orbifold model, one obtains the following boundary conditions at the string scale, M_S, in the limit of $\sin\theta\to 0$:

 © 1997 The American Physical Society

$$M_3^0 = 1.0\sqrt{3} m_{3/2}[-(3+\delta_{\rm GS})K\eta],$$

$$M_2^0 = 1.06\sqrt{3} m_{3/2}[-(-1+\delta_{\rm GS})K\eta],$$

$$M_1^0 = 1.18\sqrt{3} m_{3/2}[-(-33/5+\delta_{\rm GS})K\eta],$$

$$m_0^2 = m_{3/2}^2[-\delta_{\rm GS}K'],$$

$$A_0 = 0, \tag{1}$$

where we shall employ the one-loop numerical estimates of Ref. [2], $K = 4.6\times10^{-4}$ and $K' \equiv 1/(24\pi^2 Y) = 10^{-3}$. (The 0 subscript or superscript indicates the M_U-scale value.) In the above, $\delta_{\rm GS}$ is the Green-Schwarz mixing parameter, which preferably lies in the range 0 to -5. In the specific O-II model considered, $\delta_{\rm GS}$ would be a negative integer, with $\delta_{\rm GS} = -4, -5$ preferred. In Eq. (1), $\eta = \pm 1$, corresponding to $\sin\theta \to 0$ with $\cos\theta = \pm 1$ (i.e., $\theta \to 0, \pi$).

In Ref. [2], two sources for the B parameter were considered, labeled by B_Z and B_μ. Here, $B\mu$ is the coefficient of the $H_1 H_2$ mixing term in the scalar Higgs sector potential. (We employ the conventions for B and μ of Ref. [6].) The source of B_Z is the Giudice-Masiero mechanism [5]. It was stated that only B_μ could be present in orbifold models. More recently [3], it was realized that B_Z could also be present, and, as well, a third type of B contribution, B_λ, was discussed. In general, there could be a mixture of all three. Here, we focus on just B_Z and B_μ. A somewhat uncertain [in the sense that many additional approximations are made beyond those required for Eq. (1)] prediction for B_μ in the O-II model is

$$B_\mu^0 = m_{3/2}[-1-(1-\delta_{\rm GS}K')^{-1/2}\eta]. \tag{2}$$

If one were to adopt this prediction for B, then the value of B would be extremely large for $\eta = +1$, and only $\eta = -1$ can possibly be phenomenologically relevant. For this choice,

$$B_\mu^0 \simeq -\frac{1}{2} m_0 \sqrt{-\delta_{\rm GS}K'} \tag{3}$$

and B^0 would typically be much smaller than m_0 for the value of K' we employ. The result for B_Z^0 is very different:

$$|B_Z^0||\mu_0| = (m_0^2 + |\mu_0|^2), \tag{4}$$

which corresponds to $\tan\beta = 1$ at M_U. Because of the large number of possibilities for B we shall leave B^0 as a free parameter; it turns out to be closely related to $\tan\beta$, where $\tan\beta = v_2/v_1$ is the ratio of the vacuum expectation values of the neutral components of the Higgs doublet fields responsible for giving mass to the up- and down-type quarks, respectively. We find that $\tan\beta$ (at m_Z) near 1 is required for pure B_Z and that very large $\tan\beta$ is needed for consistency with pure B_μ.

If the model prediction for the B parameter is ignored, the sign of η becomes physically irrelevant since the overall sign of the GUT scale gaugino masses in Eq. (1) can be rotated away (since $A_0 = 0$) by an appropriate overall phase choice for the gaugino fields. (However, the opposite sign of M_3^0 relative to $M_{1,2}^0$ for $|\delta_{\rm GS}| < 3$ is physically relevant; it impacts the running of the A parameters and of B.)

We shall consider these boundary conditions within the context of the minimal supersymmetric standard model (MSSM) with exactly two Higgs doublets. This context is motivated by the fact that it is only for exactly two doublets (plus possible singlets) that the coupling constants unify without intermediate scale matter. However, it must be noted that the scale M_U at which the coupling constants unify is substantially below the string scale, M_S, at which the above boundary conditions naively apply. Thus, we shall be implicitly assuming that there is some effect, such as chiral fields in the spectrum between M_U and M_S, that compensates for this discrepancy.

Taking B^0 to be a free parameter in addition to m_0 and $\delta_{\rm GS}$, we evolve down to scales below a TeV and fix the superpotential parameter μ (which appears in the $\mu\hat{H}_1\hat{H}_2$ superpotential term) by requiring that electroweak symmetry breaking (EWSB) gives the correct value of m_Z. The sign of μ remains undetermined. In practice, it is more convenient to trade the parameter B^0 for the parameter $\tan\beta$. The top and bottom quark Yukawa couplings are constrained to yield the observed values of m_t and m_b, which we take to be $m_t(m_t) = 165$ GeV and $m_b(m_b) = 4.25$ GeV. We do not insist on $b-\tau$ Yukawa unification. The free parameters of the model are thus

$$m_0, \quad \delta_{\rm GS}, \quad \tan\beta, \quad {\rm sgn}(\mu). \tag{5}$$

We will often consider a fixed value for m_0 and plot results as a function of $\tan\beta$ and/or $\delta_{\rm GS}$. For fixed choices of m_0, $\delta_{\rm GS}$, and sgn(μ), B^0 can be viewed as a function of $\tan\beta$ and its value can be compared to the rough model predictions of Eqs. (3) and (4). We shall return to this comparison shortly.

It is useful to summarize the behavior and magnitude of the M_i^0 as a function of $-\delta_{\rm GS}$. From Eq. (1) we find the following.

(a) When $\delta_{\rm GS} \to 0$ at fixed m_0, the $|M_i|$ grow roughly as

$$[|M_1^0|, |M_2^0|, |M_3^0|] \sim \left[\frac{33}{5}, 1, 3\right]\left(\frac{\sqrt{3}Km_0}{\sqrt{-\delta_{\rm GS}K'}} \sim \frac{0.025 m_0}{\sqrt{-\delta_{\rm GS}}}\right). \tag{6}$$

(b) For $\delta_{\rm GS} = -4, -5$, as possibly preferred in the O-II model, $m_0 \gg |M_1^0| \gg |M_2^0| \gg |M_3^0|$. For $\delta_{\rm GS} = -3$, $|M_3^0| = 0$.

(c) If $-\delta_{\rm GS}$ is large (roughly $-\delta_{\rm GS} \gtrsim 30$–$40$), then the $|M_i^0|$ become approximately universal, with

$$|M_i^0| \sim \sqrt{-\delta_{\rm GS}}\,\frac{\sqrt{3}Km_0}{\sqrt{K'}} \sim 0.025 m_0 \sqrt{-\delta_{\rm GS}}. \tag{7}$$

The first important point to note is that, unless $\delta_{\rm GS}$ is extremely large ($-\delta_{\rm GS} \gtrsim 100$) or very small ($-\delta_{\rm GS} \lesssim 0.001$), the (tree-level) value of m_0 is very much larger than any of the $|M_i^0|$; this is basically due to the fact that K and K' are similar in size and have typically small one-loop magnitudes. Consequently, the squarks, sleptons, and heavier Higgs bosons (H^0, A^0, and $H^\pm$, with $m_{H^0} \sim m_{A^0} \sim m_{H^\pm}$) in this model will be much heavier than the gauginos. Further, the M_i^0 themselves are very nonuniversal unless $|\delta_{\rm GS}|$ is large. In particular, for any moderate choice of $\delta_{\rm GS}$, $|M_1^0| \gg |M_2^0|$, implying that the lightest chargino and lightest neutralino will both be winolike and nearly degenerate in mass. This will

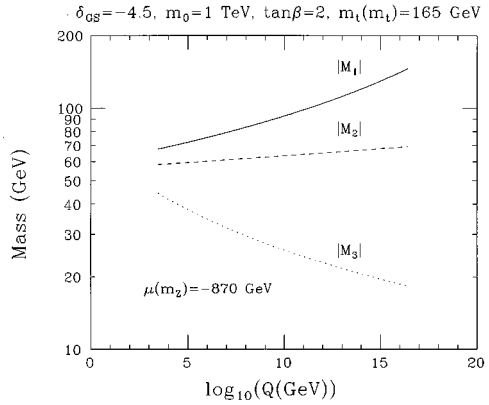

FIG. 1. Running values for the $|M_i|$ as a function of the scale Q, taking $m_0=1$ TeV, $\tan\beta=2$, $\delta_{\rm GS}=-4.5$, $m_t(m_t)=165$ GeV, and $\mathrm{sgn}(\mu)=-1$.

have important phenomenological implications. Values of $\delta_{\rm GS}\sim -3$, i.e., near the zero of $|M_3^0|$, will be physically disallowed by the requirement that the gluino cannot be the lightest supersymmetric particle.

For $\delta_{\rm GS}=-4,-5$ or thereabouts, $|M_1|\gg|M_2|\gg|M_3|$ at M_U and the $|M_i|$ approach one another as one evolves down to m_Z. This is illustrated in Fig. 1. Figure 2 illustrates the $B^0=B(M_U)$ and $\mu(m_z)$ parameter values as a function of $\tan\beta$ for $\delta_{\rm GS}=-0.1$ and -4.5. (Results for still larger $|\delta_{\rm GS}|$ are rather close to those plotted for $\delta_{\rm GS}=-4.5$.) Both B and μ evolve rather slowly as a function of scale. Note that $|\mu(m_Z)|$ is independent of the sign of μ, but that $|B^0|$ is not. The sign of B^0 is generally opposite that of μ for correct electroweak symmetry breaking. Except for $\mu>0$ and small $|\delta_{\rm GS}|$, the B^0 required by EWSB (dashed lines) crosses the approximate model prediction of Eq. (3) (indicated by the dotted lines) at high $\tan\beta$ before $\tan\beta$ exceeds the $\tan\beta\lesssim 50$ limit imposed by perturbativity for the Yukawa couplings. Clearly, the B_μ prediction of the O-II model for B^0 is generally consistent with the requirements of EWSB only if $\tan\beta$ is large. From the plots of B^0 and $|\mu|$ in Fig. 2, it is also apparent that pure B_Z is only possible if $\tan\beta$ is near 1.

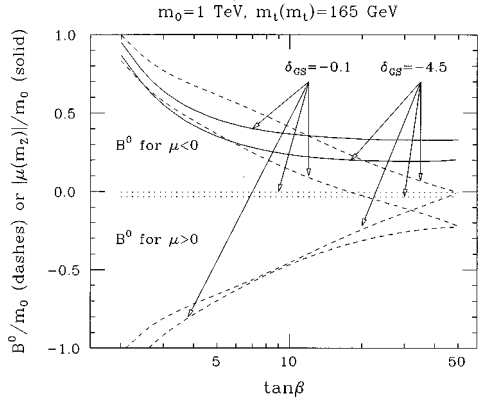

FIG. 2. Values of B^0/m_0 (dashes) and $|\mu(m_Z)|/m_0$ (solid) as a function of $\tan\beta$ for $\delta_{\rm GS}=-0.1$ and -4.5, taking $m_0=1$ TeV and $m_t(m_t)=165$ GeV. Results for $|\mu(m_Z)|$ are the same for $\mu>0$ and $\mu<0$; B^0 depends upon the sign of μ, with $B^0>0$ being favored for $\mu<0$ and vice versa. The two horizontal dotted lines are the values of B^0 predicted by Eq. (3).

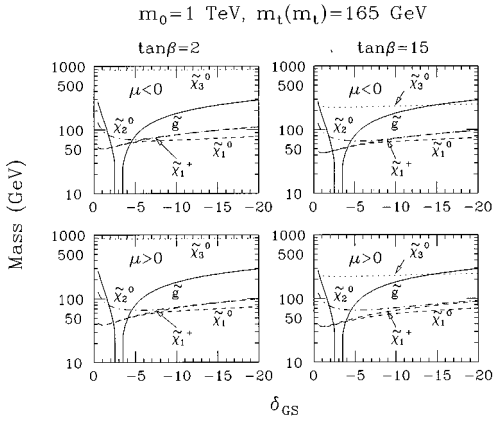

FIG. 3. Masses for the $\widetilde{\chi}_1^0$, $\widetilde{\chi}_2^0$, $\widetilde{\chi}_3^0$, $\widetilde{\chi}_1^+$, and $\widetilde{g}$ are plotted as a function of $\delta_{\rm GS}$ at $\tan\beta=2$ and 15 and for $\mu>0$ and $\mu<0$.

We note that the existence of solutions with $\mu^2>0$ (as required for correct electroweak symmetry breaking) at large $\tan\beta$ is rather sensitive to the value of $m_t(m_t)$. This is because the value of μ^2 required for EWSB drops rapidly (see Fig. 2) as $\tan\beta$ increases. For values of $m_t(m_t)\lesssim 160$ GeV (i.e., not much lower than the 165 GeV value chosen here), $\mu^2<0$ is required for correct EWSB at scale m_Z if $\tan\beta$ is large. The results presented in this paper employ one-loop renormalization-group equations; the full two-loop equations for the entire system of renormalization group equations (RGE's) are very difficult to implement. It is conceivable that μ^2 remaining positive out to large $\tan\beta$ for $m_t(m_t)=165$ GeV could be altered in the full two-loop implementation.

Typical results for the gaugino masses as a function of $\delta_{\rm GS}$ are illustrated in Fig. 3 for $\mu>0$ and $\mu<0$, taking $m_0=1$ TeV and $\tan\beta=2,15$. Note that a large value of m_0 is required for $m_{\widetilde{\chi}_1^\pm}>m_Z/2$. As discussed later, this lower bound from the CERN d^+e^- collider LEP-I data continues to apply in the present model. We observe that for $|\delta_{\rm GS}|<5$ the $\widetilde{\chi}_1^0$ and $\widetilde{\chi}_1^+$ are extremely degenerate. When this near degeneracy is present we will use the notation

$$\Delta m_{\widetilde{\chi}_1}\equiv m_{\widetilde{\chi}_1^\pm}-m_{\widetilde{\chi}_1^0},\quad m_{\widetilde{\chi}_1}\equiv m_{\widetilde{\chi}_1^\pm}\simeq m_{\widetilde{\chi}_1^0}. \tag{8}$$

The degeneracy slowly eases as $\tan\beta$ increases. Figure 4 dis-

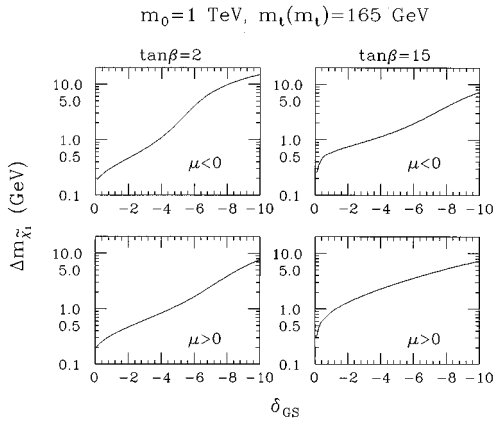

FIG. 4. The mass splitting $\Delta m_{\widetilde{\chi}_1}\equiv m_{\widetilde{\chi}_1^\pm}-m_{\widetilde{\chi}_1^0}$ as a function of $\delta_{\rm GS}$ at $\tan\beta=2$ and 15 and for $\mu>0$ and $\mu<0$.

plays the $\widetilde{\chi}_1^{\pm}$-$\widetilde{\chi}_1^0$ mass splitting in more detail. In obtaining precise values for $\Delta m_{\widetilde{\chi}_1}$ it is important to include loop corrections, the only significant such corrections being from gauge-Higgs loops. We employed the results of Refs. [7, 8]. Figure 4 shows that $\Delta m_{\widetilde{\chi}_1}$ can be as small as 150 MeV at small $|\delta_{\rm GS}|$, if $\tan\beta=2$. For $\delta_{\rm GS}\sim -5$, $\Delta m_{\widetilde{\chi}_1}$ is $\lesssim$1–2 GeV in all cases. Values of $\Delta m_{\widetilde{\chi}_1}\gtrsim 10$ GeV are only achieved for $|\delta_{\rm GS}|>10$–15, depending upon $\tan\beta$ and $\mathrm{sgn}(\mu)$. From Fig. 3, we also observe that for values of $\delta_{\rm GS}$ in the vicinity of -3, the gluino becomes the lightest supersymmetric particle.[1] Such values of $\delta_{\rm GS}$ are excluded by cosmological arguments which imply that the lightest supersymmetric particle (LSP) cannot be colored. Note that the other gauginos also have their minimum masses in the vicinity of this disallowed region. As noted in Eqs. (6) and (7), as $-\delta_{\rm GS}\to 0$ or for large $-\delta_{\rm GS}$ the $|M_i^0|$ increase away from their minimum values. Finally, we note that for very small $|\delta_{\rm GS}|$ the ratio $m_{\widetilde{g}}/m_{\widetilde{\chi}_1^{\pm}}$ reaches values as high as 6 to 7, substantially above the value $\sim$3 typical of a model with universal $|M_i^0|$ at M_U.

The near equality of $m_{\widetilde{\chi}_1^+}$ and $m_{\widetilde{\chi}_1^0}$ at lower $|\delta_{\rm GS}|$ follows from the fact that $|M_1^0|$ is large compared to $|M_2^0|$ at M_U, which implies that even though $|M_1|$ falls towards $|M_2|$ as the scale decreases, $|M_1|>|M_2|$ at m_Z. As a result, for such $\delta_{\rm GS}$, the $\widetilde{\chi}_1^0$ and the $\widetilde{\chi}_1^+$ are both primarily winos and thus have very similar mass.

In contrast to the $\widetilde{\chi}_1^+$, the $\widetilde{\chi}_2^0$ is never especially degenerate with the $\widetilde{\chi}_1^0$. At small $|\delta_{\rm GS}|$, $m_{\widetilde{\chi}_2^0}\sim|M_1|$ is substantially above $m_{\widetilde{\chi}_1^+}\sim m_{\widetilde{\chi}_1^0}\sim|M_2|$ at scale m_Z. At high $|\delta_{\rm GS}|$, as the $|M_i^0|$ approach universality, one approaches the more familiar situation where the $\widetilde{\chi}_2^0$ and $\widetilde{\chi}_1^+$ are both winos and $m_{\widetilde{\chi}_2^0}\sim m_{\widetilde{\chi}_1^+}>m_{\widetilde{\chi}_1^0}$. Also shown in Fig. 3 is $m_{\widetilde{\chi}_3^0}$. Because the $\widetilde{\chi}_2^{\pm}$, $\widetilde{\chi}_3^0$, and $\widetilde{\chi}_4^0$ are all primarily Higgsino in nature, they will have similar mass ($\sim|\mu|$).

Additional perspective on masses is provided by Fig. 5 where we give contours for $m_{\widetilde{g}}=50$–350 in steps of 50 GeV in $\delta_{\rm GS}-m_0$ parameter space. The $m_{\widetilde{g}}$ contours are independent of $\tan\beta$ and $\mathrm{sgn}(\mu)$. Also shown are the contours for $m_{\widetilde{\chi}_1^+}=47$ and 90 GeV, for $\tan\beta=2$ and $\mu<0$. Parameter space points to the left of the 47 GeV contour are excluded by LEP-I data, implying that $m_{\widetilde{g}}$ must lie above about 50 GeV. The gap region is that excluded by requiring that the $\widetilde{g}$ not be the LSP. Note that $m_{\widetilde{g}}/m_0$ is small when $|\delta_{\rm GS}|$ is not large. Thus, for example, if we assume that naturalness demands that m_0 lie below about 2 TeV, the maximum $m_{\widetilde{g}}$ that can be achieved along the $m_{\widetilde{g}}\sim m_{\widetilde{\chi}_1}$ [see Eq. (8)] border is of order 150 GeV. Even in the extreme $\delta_{\rm GS}\sim -10$, $m_0=2$ TeV corner of the plot, $m_{\widetilde{g}}\sim 375$ GeV. Large $m_{\widetilde{g}}$ values can only be achieved by taking either very small or very large $-\delta_{\rm GS}$, keeping m_0 fixed. Despite the generally small size of $m_{\widetilde{g}}$, we will see that $\widetilde{g}$ detection at a hadron collider is challenging along the $m_{\widetilde{g}}\sim m_{\widetilde{\chi}_1}$ boundary. As one moves away from the $m_{\widetilde{g}}\sim m_{\widetilde{\chi}_1}$ boundary, discovery of the $\widetilde{g}$ becomes easier, eventually approaching expectations for the canonical universal boundary condition scenarios.

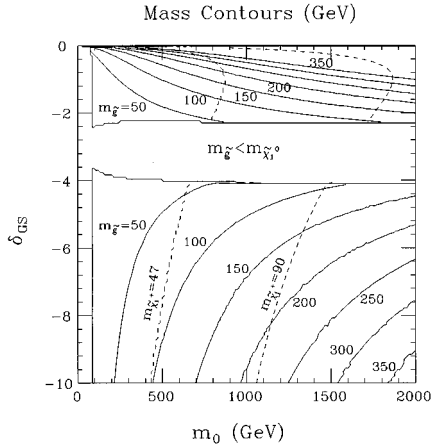

FIG. 5. Gluino mass contours in $\delta_{\rm GS}-m_0$ parameter space. The gluino contours are independent of $\tan\beta$ and $\mathrm{sgn}(\mu)$. Also shown are the corresponding $m_{\widetilde{\chi}_1^+}=47$ and 90 GeV contours for $\tan\beta=2$ and $\mu<0$. The $\widetilde{\chi}_1^+$ contour depends only weakly on $\tan\beta$ and $\mathrm{sgn}(\mu)$.

The masses for all sleptons, heavy Higgs bosons, and squarks are of the order of m_0. As seen in Figs. 3 and 5, unless $|\delta_{\rm GS}|$ is very large or very small, m_0 is much larger than the gaugino masses. Consequently, for the $\sin\theta\to 0$ O-II model being considered it is likely that the gauginos will be the most abundantly produced SUSY particles, and they would probably provide the first observed SUSY signals. The next section is devoted to a discussion of the search strategies required, emphasizing the difficulties that arise in $\widetilde{\chi}_1^{\pm}$ detection at an e^+e^- collider when the $\widetilde{\chi}_1^+$ and $\widetilde{\chi}_1^0$ are closely degenerate and in discovering the gluino at a hadron collider when $m_{\widetilde{g}}$ is close to $m_{\widetilde{\chi}_1}\equiv m_{\widetilde{\chi}_1^{\pm}}\simeq m_{\widetilde{\chi}_1^0}$.

II. PHENOMENOLOGY

In this section we discuss SUSY discovery strategies for the $\sin\theta\to 0$ O-II model. Because of the special features of the mass spectrum, SUSY discovery can be substantially more difficult than in models where the gaugino masses are universal at M_U. Universality at M_U implies the hierarchy

$$|M_1|\sim\frac{1}{2}|M_2|\sim\frac{1}{6}|M_3|<|\mu|, \tag{9}$$

at scale m_Z. In this case, the $\widetilde{\chi}_1^0$ LSP is a bino and its mass, $\sim|M_1|$, is significantly lower than the masses of the $\widetilde{\chi}_1^+$ and $\widetilde{\chi}_2^0$, $\sim|M_2|$, which is substantially below $m_{\widetilde{g}}\sim|M_3|$. As a consequence, the $\widetilde{g}$ typically decays to the $\widetilde{\chi}_1^+$ or $\widetilde{\chi}_1^0$ plus a pair of energetic quark jets and the $\widetilde{\chi}_1^+$ decays to the $\widetilde{\chi}_1^0$ by emitting a $\ell\nu$ or $q'\overline{q}$ pair with significant energy. The substantial energy carried by the decay products implies that production of the lightest chargino and of the gluino will be associated with both energetic jets/leptons and substantial missing energy, a combination that is generally easily separated from backgrounds at an e^+e^- or hadron collider operating at high enough energy and luminosity.

[1]We always discuss and plot $m_{\widetilde{g}}$(pole). Thus, for example, even though $|M_3|$ lies below $|M_2|$ in Fig. 1, the pole value of $m_{\widetilde{g}}$ is greater than $m_{\widetilde{\chi}_1^0}$. For the parameters of the plot, $m_{\widetilde{g}}$(pole)$\sim$66 GeV while $m_{\widetilde{\chi}_1^0}\sim$62.4 GeV.

In the O-II model, SUSY detection need not be so straightforward. We have already noted that it is natural for $\Delta m_{\widetilde{\chi}_1}$ to be sufficiently small that the final-state quarks or lepton from $\widetilde{\chi}_1^\pm$ decay to $\widetilde{\chi}_1^0$ are very soft and not easily observed. We will also find that the $\widetilde{\chi}_1^\pm$'s lifetime is not likely to be sufficiently long that it will appear as a stable particle track in the detector—short tracks in a vertex detector are, however, a distinct possibility. Less automatic, but also possible, is degeneracy of $m_{\widetilde{g}}$ with $m_{\widetilde{\chi}_1} \equiv m_{\widetilde{\chi}_1^\pm} \simeq m_{\widetilde{\chi}_1^0}$. The jets from $\widetilde{g}$ decay to $\widetilde{\chi}_1^\pm$ or $\widetilde{\chi}_1^0$ would then be very soft and difficult to detect.

At an e^+e^- collider, small $\Delta m_{\widetilde{\chi}_1}$ leads to difficulty in detecting $e^+e^- \to \widetilde{\chi}_1^+\widetilde{\chi}_1^-$. Indeed, the techniques discussed for isolating the $\widetilde{\chi}_1^+\widetilde{\chi}_1^-$ signal at LEP-II (i.e., above the Z pole) have good efficiency only for[2] $\Delta m_{\widetilde{\chi}_1} \gtrsim 10$ GeV. Most likely, it would be necessary to employ other reactions to first discover SUSY. One possibility is the much smaller $e^+e^- \to \widetilde{\chi}_1^0\widetilde{\chi}_2^0, \widetilde{\chi}_2^0\widetilde{\chi}_2^0$ production processes, in which the $\widetilde{\chi}_2^0$ would generally yield energetic and visible decays products, given that the smallest $m_{\widetilde{\chi}_2^0} - m_{\widetilde{\chi}_1^0}$ mass difference values are of order 5–10 GeV (for $\delta_{\rm GS}$ between -6 and -9). Another is $e^+e^- \to \gamma\widetilde{\chi}_1^+\widetilde{\chi}_1^-$ production in which the nearly or completely invisible $\widetilde{\chi}_1^+\widetilde{\chi}_1^-$ pair is tagged by detecting the hard γ. This latter was investigated in Ref. [10], and will be reviewed shortly.

At a hadron collider, if $m_{\widetilde{g}}$ is close to $m_{\widetilde{\chi}_1}$, the softness of the jets in $\widetilde{g}$ decay implies that the usual procedures for isolating gluino pair production at a hadron collider by tagging missing energy *and* jets may yield a rather weak signal. Further, if the ℓ from $\widetilde{\chi}_1^\pm$ decay is soft due to small $\Delta m_{\widetilde{\chi}_1}$ then (a) the like-sign dilepton signature for $\widetilde{g}\widetilde{g}$ production that derives from $\widetilde{g}\widetilde{g} \to \widetilde{\chi}_1^\pm\widetilde{\chi}_1^\pm + \text{jets}$ followed by $\widetilde{\chi}_1^\pm\widetilde{\chi}_1^\pm \to \ell^\pm\ell^\pm \not{E}_T$ will be difficult to extract; and, (b) the trilepton signature for $\widetilde{\chi}_1^\pm\widetilde{\chi}_2^0$ production will be hard to observe.

Thus, it is clear that the O-II model leads to a situation where the techniques and prospects for detecting SUSY must be reevaluated.

A. Lifetime and branching ratios of the $\widetilde{\chi}_1^+$

From the above discussion, it is clear that important ingredients in the phenomenology of SUSY detection in the O-II model context are the branching ratios and lifetime of the $\widetilde{\chi}_1^+$. These have been computed using PCAC (partial conservation of axial-vector current) style techniques as described in Appendix A. We find that both the branching ratios and the lifetime depend almost entirely upon the mass difference $\Delta m_{\widetilde{\chi}_1} = m_{\widetilde{\chi}_1^\pm} - m_{\widetilde{\chi}_1^0}$. Dependence upon $\tan\beta$ and μ is minimal. Results for the lifetime τ and for the important branching ratios of the $\widetilde{\chi}_1^+$ are plotted in Fig. 6. We observe that $\tau \gtrsim 10^{-10}$ s for $\Delta m_{\widetilde{\chi}_1} \lesssim 300$ MeV, i.e., $|\delta_{\rm GS}| \lesssim 0.5$–2 depending upon sgn($\mu$) and $\tan\beta$ (see Fig. 4). For $\tau \sim 10^{-10}$ s, the track of the $\widetilde{\chi}_1^+$ would be visible in a vertex detector; for $\Delta m_{\widetilde{\chi}_1} \lesssim 150$ MeV τ becomes so long that the $\widetilde{\chi}_1^\pm$ would appear as a charged ''stable'' particle track.

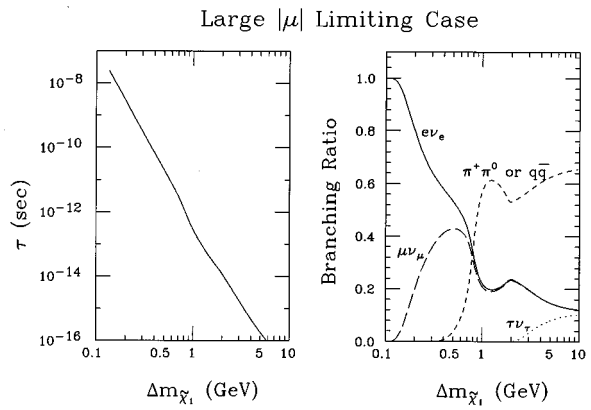

FIG. 6. We plot the lifetime and the relevant branching ratios for the $\widetilde{\chi}_1^+$ as a function of $\Delta m_{\widetilde{\chi}_1} \equiv m_{\widetilde{\chi}_1^\pm} - m_{\widetilde{\chi}_1^0}$. A single curve represents the $\pi^+\pi^0\widetilde{\chi}_1^0$ or $q'\overline{q}\widetilde{\chi}_1^0$ branching ratio; the transition between the two different calculations of the hadronic mode decays is made at $\Delta m_{\widetilde{\chi}_1} = 2$ GeV.

For $\Delta m_{\widetilde{\chi}_1} \lesssim 500$ MeV, $\widetilde{\chi}_1^+ \to \ell^+\nu_\ell\widetilde{\chi}_1^0$ ($\ell = e,\mu$) is the only kinematically allowed decay mode. As the mass difference increases, $\widetilde{\chi}_1^+ \to \pi^+\widetilde{\chi}_1^0$ opens up but is strongly suppressed,[3] followed by $\widetilde{\chi}_1^+ \to \rho^+\widetilde{\chi}_1^0 \to \pi^+\pi^0\widetilde{\chi}_1^0$, with these channels eventually merging into $\widetilde{\chi}_1^+ \to q'\overline{q}\widetilde{\chi}_1^0$. For still larger mass difference, $\widetilde{\chi}_1^+ \to \tau^+\nu_\tau\widetilde{\chi}_1^0$ becomes kinematically allowed. The $\ell^+\nu\widetilde{\chi}_1^0$ ($\ell = e$, or μ, or eventually τ) are important channels, even after the general $\widetilde{\chi}_1^+ \to q'\overline{q}\widetilde{\chi}_1^0$ channels are open.

B. Constraints from LEP and LEP 1.5

We note that the $\widetilde{\chi}_1^\pm$ cannot be lighter than $m_Z/2$. We have explicitly checked that the $Z \to \widetilde{\chi}_1^+\widetilde{\chi}_1^-$ decays would have been noticed either as an invisible width contribution or through an enhancement in the total Z width. This statement applies for masses up to within a fraction of a GeV of $m_Z/2$. The $Z \to \widetilde{\chi}_1^0\widetilde{\chi}_1^0, \widetilde{\chi}_1^0\widetilde{\chi}_2^0, \widetilde{\chi}_2^0\widetilde{\chi}_2^0$ decays have much smaller widths (due to the small Higgsino component of the $\widetilde{\chi}_1^0$ and $\widetilde{\chi}_2^0$) and do not provide useful direct limits. Implicit limits on $m_{\widetilde{\chi}_1^0}$ associated with the $m_{\widetilde{\chi}_1^\pm} \gtrsim m_Z/2$ limit depend upon $\delta_{\rm GS}$. For small $|\delta_{\rm GS}|$ the degeneracy $m_{\widetilde{\chi}_1^0} \simeq m_{\widetilde{\chi}_1^\pm}$ implies that $m_{\widetilde{\chi}_1^0} \gtrsim m_Z/2$ as well. However, for large $|\delta_{\rm GS}|$ the $\widetilde{\chi}_1^0$ is significantly lighter than the $\widetilde{\chi}_1^\pm$, and $m_{\widetilde{\chi}_1^0} < m_Z/2$ is allowed. At large $|\delta_{\rm GS}|$, such that $\Delta m_{\widetilde{\chi}_1} \gtrsim 5$–10 GeV, the LEP 1.5 limit of $m_{\widetilde{\chi}_1^\pm} \gtrsim 65$ GeV applies (see next section for further discussion). The lowest $\widetilde{\chi}_1^0$ mass consistent with this limit for $|\delta_{\rm GS}| \lesssim 20$ is $m_{\widetilde{\chi}_1^0} = 41$ GeV (corresponding to $m_0 = 520$ GeV at $\delta_{\rm GS} = -20$).

[2] In a recent paper [9], the L3 Collaboration mentions a specialized technique employed at $\sqrt{s} \sim 130$–140 GeV for retaining some 5–10 % efficiency down to $\Delta m_{\widetilde{\chi}_1} = 5$ GeV, but details are not given.

[3] This is because the $\widetilde{\chi}_1^+\widetilde{\chi}_1^0 W^-$ coupling is almost purely vector in nature, whereas the $\widetilde{\chi}_1^+ \to \pi^+\widetilde{\chi}_1^0$ decay proceeds via the axial-vector current.

C. SUSY discovery at e^+e^- colliders

Let us begin by considering the neutralino and chargino pair production cross sections. As the $\sqrt{s}$ of the machine increases, the first channels to open up will be those for the lighter eigenstates:

$$e^+e^- \to \gamma^*, \quad Z^* \to \tilde{\chi}_1^+ \tilde{\chi}_1^-,$$

$$e^+e^- \to Z^* \to \tilde{\chi}_1^0\tilde{\chi}_1^0, \tilde{\chi}_1^0\tilde{\chi}_2^0, \tilde{\chi}_2^0\tilde{\chi}_2^0. \tag{10}$$

If $|\delta_{\rm GS}|$ is not too large, the $\tilde{\chi}_1^0$ and $\tilde{\chi}_2^0$ are primarily wino and bino, respectively, with weak couplings to the Z, and the latter neutralino pair cross sections are always much smaller than the $\tilde{\chi}_1^+\tilde{\chi}_1^-$ cross section.[4] As $\sqrt{s}$ increases,

$$e^+e^- \to \tilde{\chi}_1^\pm \tilde{\chi}_2^\mp, \quad e^+e^- \to \tilde{\chi}_{1,2}^0 \tilde{\chi}_{3,4}^0 \tag{11}$$

become kinematically allowed. When allowed, the latter gaugino-Higgsino (light-heavy) neutralino pair cross sections are larger than the gaugino-gaugino (light-light) neutralino pair cross sections due to the large Higgsino components of the heavy neutralinos. At still higher $\sqrt{s}$, typically above (below) 500 GeV if tanβ is small (large), the

$$e^+e^- \to \tilde{\chi}_2^+ \tilde{\chi}_2^-, \quad e^+e^- \to \tilde{\chi}_{3,4}^0 \tilde{\chi}_{3,4}^0, \tag{12}$$

processes become possible. When allowed, the Higgsino-Higgsino (heavy-heavy) neutralino pair cross sections are comparable to chargino pair cross sections.

As $-\delta_{\rm GS}$ increases in magnitude, the B ino or W ino content of the $\tilde{\chi}_1^0$ and $\tilde{\chi}_2^0$ becomes more mixed, but the general cross section expectations are not greatly altered since μ is always sufficiently large that it is the $\tilde{\chi}_2^+$, $\tilde{\chi}_3^0$, and $\tilde{\chi}_4^0$ which remain primarily Higgsino.

The relevant cross sections are illustrated for $\sqrt{s}=500$ GeV in Figs. 7 and 8. In Fig. 7 the gaps in $-\delta_{\rm GS}$ are where $m_{\tilde{g}}$ falls below 120 GeV, which includes the region where the gluino would be the LSP. The 120 GeV lower limit is a rough characterization of the bound from Fermilab Tevatron data in this model. A detailed examination of Fermilab Tevatron predictions in a later section shows that the actual bound varies significantly as a function of $-\delta_{\rm GS}$. For example, values of $m_{\tilde{g}}$ below 100 GeV are still allowed by current analyses if $m_{\tilde{g}} \sim m_{\tilde{\chi}_1}$, as happens in two narrow bands within the gap region (see Fig. 3).

As anticipated, the $\tilde{\chi}_1^+\tilde{\chi}_1^-$ cross section is far and away the largest, but for $-\delta_{\rm GS}<7$–10 can be quite difficult to see by virtue of the softness of the $\tilde{\chi}_1^\pm$ decay products. However, the $\tilde{\chi}_2^0\tilde{\chi}_{1,2}^0$ cross section and the various gaugino-Higgsino cross sections can be kinematically allowed and large enough to be observable. For all these latter processes the final state should contain some energetic leptons or jets in association with a large amount of missing energy and should be easily detected if the event rate is adequate. For the target yearly luminosity of $L=50$ fb^{-1} at $\sqrt{s}=500$ GeV, one can probably be sensitive to a raw cross section as small as 10^{-3} pb (yielding 50 events before cuts) in such final states. Figure 7 shows that if $-\delta_{\rm GS}$ is not below $\sim$0.05, then at least one of these visible final states will have adequate cross section.

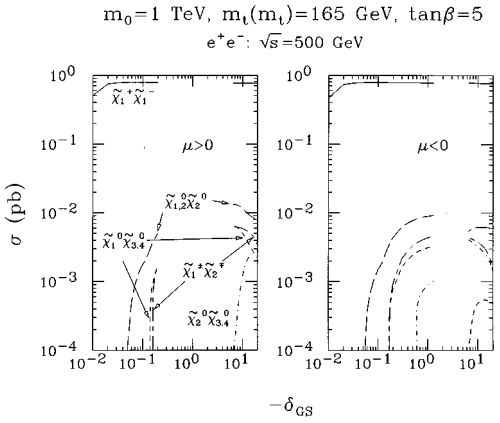

FIG. 7. Neutralino and chargino pair cross sections in e^+e^- collisions at $\sqrt{s}=500$ GeV as a function of $-\delta_{\rm GS}$, taking $m_0=1$ TeV and tan$\beta=5$. Results are displayed for both signs of μ. The gap in $-\delta_{\rm GS}$ is where $m_{\tilde{g}} \leqslant 120$ GeV ($\mu<0$), a very rough limit from Tevatron data, or $m_{\tilde{\chi}_1^\pm}<45$ GeV ($\mu>0$), as excluded by LEP1. The legend is solid, $\tilde{\chi}_1^+\tilde{\chi}_1^-$; long dashes, $\tilde{\chi}_2^0\tilde{\chi}_{1,2}^0$; short dashes, $\tilde{\chi}_1^0\tilde{\chi}_{3,4}^0$; dot-dashed, $\tilde{\chi}_2^0\tilde{\chi}_{3,4}^0$; long-dash–short-dashed, $\tilde{\chi}_1^\pm\tilde{\chi}_2^\mp$.

The first visible final states to become accessible as $-\delta_{\rm GS}$ increases are $\tilde{\chi}_1^0\tilde{\chi}_2^0$ and $\tilde{\chi}_2^0\tilde{\chi}_2^0$. These are not kinematically allowed at small $-\delta_{\rm GS}$ since $m_{\tilde{\chi}_2^0}$ becomes a factor of 3 larger than $m_{\tilde{\chi}_1}$, and is growing $\propto 1/\sqrt{-\delta_{\rm GS}}$ [see Eq. (6)]. The next channels to open up as $-\delta_{\rm GS}$ increases are $\tilde{\chi}_1^0\tilde{\chi}_{3,4}^0$ and $\tilde{\chi}_1^\pm\tilde{\chi}_2^\mp$. The thresholds for these two final states are very similar due to the degeneracies $m_{\tilde{\chi}_1^0} \sim m_{\tilde{\chi}_1^\pm}$ and $m_{\tilde{\chi}_3^0} \sim m_{\tilde{\chi}_4^0} \sim m_{\tilde{\chi}_2^\pm}$. The cross sections are of limited magnitude because

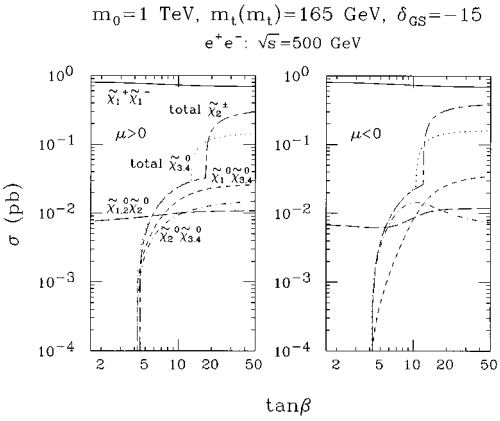

FIG. 8. Neutralino and chargino pair cross sections in e^+e^- collisions at $\sqrt{s}=500$ GeV as a function of tanβ, taking $m_0=1$ TeV and $\delta_{\rm GS}=-15$. Results are displayed for both signs of μ. The legend is solid, $\tilde{\chi}_1^+\tilde{\chi}_1^-$; long-dashed, $\tilde{\chi}_2^0\tilde{\chi}_{1,2}^0$; short-dashed, $\tilde{\chi}_1^0\tilde{\chi}_{3,4}^0$; dot-dashed, $\tilde{\chi}_2^0\tilde{\chi}_{3,4}^0$; long-dash–short-dashed, $\tilde{\chi}_1^\pm\tilde{\chi}_2^\mp + \tilde{\chi}_2^\pm\tilde{\chi}_2^\mp$; dots, $\tilde{\chi}_1^0\tilde{\chi}_{3,4}^0 + \tilde{\chi}_2^0\tilde{\chi}_{3,4}^0 + \tilde{\chi}_{3,4}^0\tilde{\chi}_{3,4}^0$.

[4]Our cross-section results include slepton and sneutrino exchanges in the t and u channels; see Ref. [11] for explicit expressions. However, these diagrams are suppressed for a $\sqrt{s} \leqslant 500$ GeV collider by the large selectron and sneutrino masses deriving from the large magnitude of m_0 (when $|\delta_{\rm GS}|$ is not extremely large).

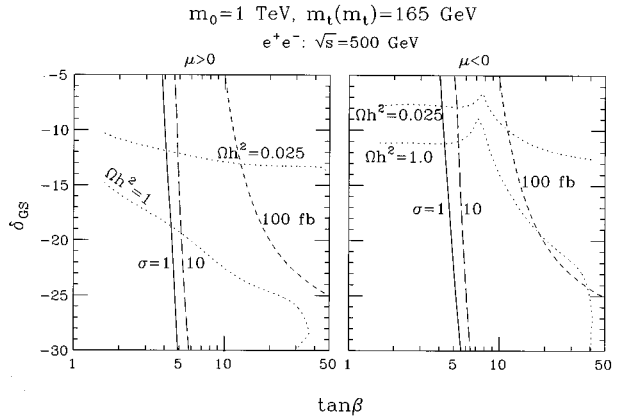

FIG. 9. Contours of constant σ [Eq. (13)] in $\tan\beta - \delta_{\rm GS}$ parameter space for $m_0=1$ TeV and $\sqrt{s}=500$ GeV. Also shown (dots) are the $\Omega h^2=1$ and 0.025 contours, see Sec. II E.

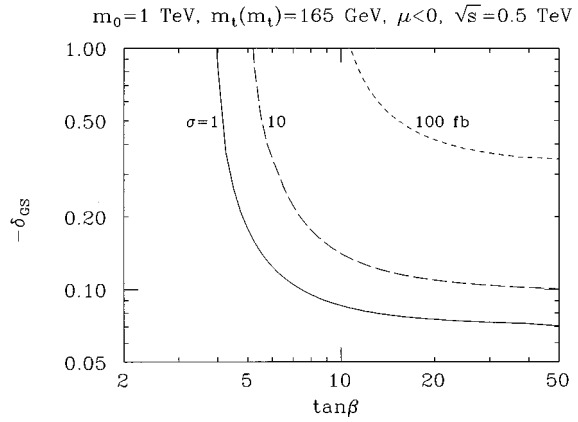

FIG. 10. Contours of constant σ [Eq. (13)] in the small $-\delta_{\rm GS}$ portion of $\tan\beta - \delta_{\rm GS}$ parameter space for $m_0=1$ TeV and $\sqrt{s}=500$ GeV.

they are only non-zero to the extent that there is some Higgsino-gaugino mixing in the mass eigenstate compositions. As $\tan\beta$ increases, Fig. 2 shows that $|\mu|$ decreases substantially, implying that the Higgsino states become lighter (see Fig. 3). This also implies greater gaugino-Higgsino mixing. Thus, as seen in Fig. 8, there is a $\tan\beta$ threshold in the $\tan\beta \gtrsim 10$–15 region where the total $\widetilde{\chi}_2^\pm$ and total $\widetilde{\chi}_3^0, \widetilde{\chi}_4^0$ cross sections suddenly increase due to the fact that the Higgsino states become light enough that they can also be pair produced at $\sqrt{s}=500$ GeV. Since the $Z \to$ Higgsino +Higgsino coupling is large, the Higgsino pair cross sections are comparable to the chargino-pair cross section. Although the $\widetilde{\chi}_3^0$ and $\widetilde{\chi}_4^0$ are primarily Higgsino in nature, their SU(2) gaugino content is generally sufficient that their dominant decay is to $W^\pm \widetilde{\chi}_1^\mp$, rather than to $h^0 \widetilde{\chi}_1^0, h^0 \widetilde{\chi}_2^0$ (where h^0 is the light *CP*-even Higgs boson) that would dominate if they were pure Higgsino.

In Fig. 9, we present contours of

$$\sigma \equiv \sum_i \left[\sigma(\widetilde{\chi}_i^0 \widetilde{\chi}_3^0) + \sigma(\widetilde{\chi}_i^0 \widetilde{\chi}_4^0) + \sigma(\widetilde{\chi}_i^\pm \widetilde{\chi}_2^\mp) \right] \qquad (13)$$

in the $\tan\beta - \delta_{\rm GS}$ parameter plane for a $\sqrt{s}=500$ GeV e^+e^- collider. Detection of at least one of the heavier neutralino or chargino states is important as a means for determining $|\mu|$ (from the fact that the states typically have mass $\sim|\mu|$), thereby allowing a check of the consistency of electroweak symmetry breaking. Figure 9 focuses on the $-\delta_{\rm GS} \gtrsim 5$ domain. As previously noted, for increasing $\tan\beta$ the value of $|\mu|$ declines and the Higgsino masses decrease. Thus, σ will first become nonzero when gaugino+Higgsino production becomes possible, with a second very rapid increase as one crosses the Higgsino+Higgsino threshold. Figure 9 shows that the gaugino+Higgsino threshold lies at $\tan\beta \sim 5$ for $m_0=1$ TeV. For $\tan\beta \gtrsim 5$, $\sigma \gtrsim 1$ fb (implying $\gtrsim 50$ events) and detection of the heavy inos should be possible. As noted earlier, $\widetilde{\chi}_3^0, \widetilde{\chi}_4^0$ will tend to decay to $W^\pm \widetilde{\chi}_1^\mp$. The $\widetilde{\chi}_2^\pm$ will decay primarily to $Z\widetilde{\chi}_1^\pm$ or $W^\pm \widetilde{\chi}_1^0$, $W^\pm \widetilde{\chi}_2^0$. Since the thresholds for the gaugino+Higgsino final states are very steep, σ rises to 10 fb, implying 500 events, already by $\tan\beta \sim 6$–7. However, since σ is the sum over a number of modes, 500 events might still not be enough to make a precise determination of the masses of the $\widetilde{\chi}_2^\pm$, $\widetilde{\chi}_3^0$, and $\widetilde{\chi}_4^0$ and other model parameters to which the cross sections are sensitive. For this, $\sigma \sim 100$ fb (5000 events divided up among the channels) might be required. This level of cross section is generally only achieved when Higgsino+Higgsino pair production is possible, which typically requires fairly large $\tan\beta$. The $\sigma=100$ fb contour in Fig. 9 is close to the Higgsino +Higgsino threshold.

These same σ contours are displayed for small $-\delta_{\rm GS}$ in Fig. 10. As for larger $-\delta_{\rm GS}$, the $\sigma=1$ fb contour is more or less defined by the onset of gaugino+Higgsino production, and the $\sigma=100$ fb contour by the Higgsino+Higgsino threshold. Note that at small $-\delta_{\rm GS}$ the masses of all the inos become large and ino pair production is not allowed for $\sqrt{s}=500$ GeV if $m_0=1$ TeV. However, if $-\delta_{\rm GS}$ is small then m_0, which sets the scale for all masses in this model, can be lowered substantially before $m_{\widetilde{\chi}_1^\pm}$ falls below the LEP limit of 47 GeV.

1. Using photon tagging to detect $\widetilde{\chi}_1^\pm \widetilde{\chi}_1^\mp$ pair production

The most delicate question is whether $\widetilde{\chi}_1^+ \widetilde{\chi}_1^-$ production is observable when $\Delta m_{\widetilde{\chi}_1}$ is small. For sufficiently small $\Delta m_{\widetilde{\chi}_1}$ ($\lesssim 300$ MeV), $\tau \gtrsim 10^{-10}$ s and the corresponding $\gtrsim 3$ cm tracks of the $\widetilde{\chi}_1^+$ and $\widetilde{\chi}_1^-$ might be visible in a vertex detector. Perhaps the experiments at LEP could isolate such events from backgrounds. For large enough $\Delta m_{\widetilde{\chi}_1}$, the leptons from the $\widetilde{\chi}_1^+$ and $\widetilde{\chi}_1^-$ decays become visible as their momenta spectra extend out beyond $\not{p}_T \gtrsim 1$ GeV; the required $\Delta m_{\widetilde{\chi}_1}$ depends upon $m_{\widetilde{\chi}_1^\pm}$ and $\sqrt{s}$. Still, it is problematical that events with such soft leptons could be isolated from two-photon backgrounds and the like. In particular, for small $\Delta m_{\widetilde{\chi}_1}$, the final states arising in $e^+e^- \to \widetilde{\chi}_1^+ \widetilde{\chi}_1^-$ production and decay are similar (i.e., contain leptons and missing energy) to those appearing in $\gamma\gamma \to \tau^+\tau^-$ production and decay. This latter background will be very large and difficult to overcome, even if the chargino pair events can be triggered on. There are ongoing analyses by the LEP experimental groups of their sensitivity to $\widetilde{\chi}_1^+ \widetilde{\chi}_1^-$ production when $\Delta m_{\widetilde{\chi}_1}$ is small. Similar analyses at Next Linear Collider (NLC) energies are also needed. There, the leptons are some-

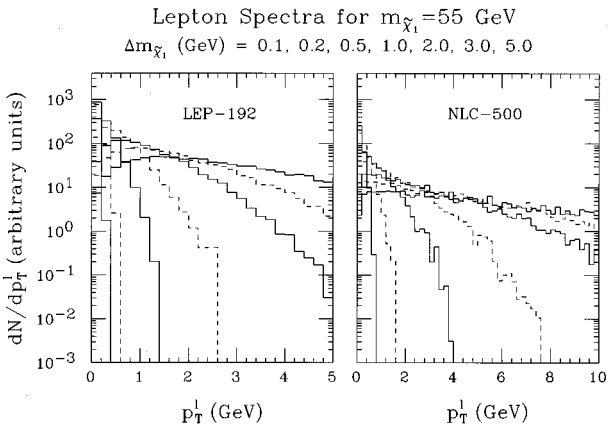

FIG. 11. $dN/dp_T^{\not\ell}$ vs $p_T^{\not\ell}$ for the soft leptons in $e^+e^-\to\gamma\tilde{\chi}_1^+\tilde{\chi}_1^-$ followed by $\tilde{\chi}_1^\pm\to\ell\nu\tilde{\chi}_1^0$ in arbitrary units, taking $m_{\tilde{\chi}_1}\equiv m_{\tilde{\chi}_1^\pm}=55$ GeV and $\Delta m_{\tilde{\chi}_1}\equiv m_{\tilde{\chi}_1^\pm}-m_{\tilde{\chi}_1^0}$ values of 0.1, 0.2, 0.5, 1, 2, 3, and 5 GeV. Results are given for LEP operating at $\sqrt{s}=192$ GeV and NLC at $\sqrt{s}=500$ GeV.

what harder for given values of $\Delta m_{\tilde{\chi}_1}$ and $m_{\tilde{\chi}_1}$ because of the higher energy, but the detector has a larger magnetic field (designed to curl up the soft leptons from beamsstrahlung and related sources). Because of the detailed level of experimental simulation required to address these questions, we will not pursue detection of $e^+e^-\to\tilde{\chi}_1^+\tilde{\chi}_1^-$ production at small $\Delta m_{\tilde{\chi}_1}$ further in this paper.

In Ref. [10] we examined $e^+e^-\to\gamma\tilde{\chi}_1^+\tilde{\chi}_1^-$ production to see if a signal could be observed above background at LEP-II and the NLC. Here a hard-photon tag provides a trigger for the presence of the $\tilde{\chi}_1^+\tilde{\chi}_1^-$ pair. We found that the range of $m_{\tilde{\chi}_1^\pm}$ accessible via this final state depends greatly upon whether the $\tilde{\chi}_1^\pm$ decays are in any way visible. The ability to detect a track in the vertex detector and/or *any* $\tilde{\chi}_1^+$ decay product would greatly enhance the significance of the signal. This is because $e^+e^-\to\gamma\nu\overline{\nu}$ (via γZ^*) becomes a very large background if the $\tilde{\chi}_1^\pm$ decay invisibly. Note that the threshold for experimental visibility of the $\tilde{\chi}_1^\pm$ decays might be quite different for different decay modes. A good electromagnetic calorimeter might be able to detect the photons from π^0 decay in $\tilde{\chi}_1^+\to\tilde{\chi}_1^0\pi^+\pi^0$ even if the π^0 is almost at rest; unfortunately, $BR(\tilde{\chi}_1^+\to\tilde{\chi}_1^0\pi^+\pi^0)$ is $\gtrsim$10% only for $\Delta m_{\tilde{\chi}_1}\gtrsim 700$ MeV, reaching a peak at $\sim$1 GeV, well above the ρ resonance (since the phase space for $\tilde{\chi}_1^+\to\tilde{\chi}_1^0\rho$ vanishes for $\Delta m_{\tilde{\chi}_1}=m_\rho$). In contrast, soft charged particles may not reach the calorimeter in the presence of a magnetic field. Because the average energy of these soft charged particles increases in going from LEP energy to NLC energy (keeping $m_{\tilde{\chi}_1^\pm}$ and $\Delta m_{\tilde{\chi}_1}$ fixed) it is not clear that this difficulty will be more severe at the NLC than at LEP, despite the previously mentioned higher magnetic field of the NLC detector.

In order to provide a more quantitative picture of the difficulty of seeing the soft leptons coming from the $\tilde{\chi}_1^+\tilde{\chi}_1^-$ pair, we present in Fig. 11 the $p_T^{\not\ell}$ spectra deriving from $\tilde{\chi}_1^\pm\to\ell\nu\tilde{\chi}_1^0$ decays in the $\gamma\tilde{\chi}_1^+\tilde{\chi}_1^-$ final state for a variety of $\Delta m_{\tilde{\chi}_1}$ values, taking $m_{\tilde{\chi}_1^\pm}=55$ GeV. We see, for example, that to observe leptons in a significant fraction of the events when $\Delta m_{\tilde{\chi}_1}\sim 0.5$ GeV, it is necessary to have good efficiency down to at least 0.7 GeV (2 GeV) at LEP-192 (NLC-500). These lepton spectra become still softer as $m_{\tilde{\chi}_1^\pm}$ increases keeping $\Delta m_{\tilde{\chi}_1}$ fixed. For example, at NLC-500 the lepton spectra for $m_{\tilde{\chi}_1^\pm}=175$ GeV typically terminate at about 1/2 the maximum value found for $m_{\tilde{\chi}_1^\pm}=55$ GeV, keeping a fixed $\Delta m_{\tilde{\chi}_1}$ value. It will be important for the experimental groups to study how well they can do and if there are any detector changes that might increase their sensitivity to soft leptons.

If the $\gamma\nu\overline{\nu}$ background cannot be eliminated by tagging the soft decay products of the $\tilde{\chi}_1^\pm$, then we must consider the best strategy for isolating the $\gamma\tilde{\chi}_1^+\tilde{\chi}_1^-$ signal in its presence. At the same time, we must be careful to avoid additional backgrounds, the most dangerous being that from $e^+e^-\to e^+e^-\gamma$, where both the final e^+ and e^- disappear down the beam hole.

In the study of Ref. [10], we found a very effective procedure for eliminating the $e^+e^-\to e^+e^-\gamma$ background. We begin by requiring a photon tag with $p_T^\gamma\geq p_T^{\gamma\,\min}=10$ GeV and $10°\leq\theta_\gamma\leq 170°$, where θ_γ is the angle of the photon with respect to the beam axis. This guarantees that the photon enters a typical detector and will have an accurately measured momentum. We define $\gamma+\not{E}_T$ events by requiring that any other particle appearing in the 10° to 170° angular range must have energy less than $E^{\max}$, where $E^{\max}$ is detector dependent, but presumably no larger than a few GeV. Kinematics can be used to show that we can then eliminate the $e^+e^-\to e^+e^-\gamma$ background by vetoing events containing an e^+ or e^- with $E>50$ GeV and angle $\theta_{\min}\leq\theta_e\leq 10°$ with respect to either beam axis, or with $E>E^{\max}$ and $10°\leq\theta_e\leq 170°$, *provided* $p_T^{\gamma\,\min}\gtrsim\sqrt{s}\,\sin\theta_{\min}(1+\sin\theta_{\min})^{-1}$ (assuming $E^{\max}$ is not larger than a few GeV). For $p_T^{\gamma\,\min}=10$ GeV, this means that we must instrument the beam hole down to $\theta_{\min}=1.17°$. In fact, instrumentation and vetoing will be possible down to $\theta_{\min}=0.72°$ [12], implying that $p_T^{\gamma\,\min}$ could be lowered to $\sim$6.2 GeV without contamination from the $e^+e^-\to e^+e^-\gamma$ background. At LEP-192, beam hole coverage down to about 3.1° is needed when using a $p_T^{\gamma\,\min}=10$ GeV cut.

For chargino masses above $m_Z/2$, the key observation for reducing the background from $\gamma\nu\overline{\nu}$ and determining the chargino mass is to note that the missing mass $m_{Z\star}\equiv[(p^{e^+}+p^{e^-}-p^\gamma)^2]^{1/2}$ can be very accurately reconstructed.[5] For

[5]We are uncertain as to the extent to which beamstrahlung might impact our ability to compute the true $Z^\star$ system mass. Since most beamstrahlung involves radiation of just one hard photon along the beam line, the $m_{Z^\star}$ computed as above would correspond to the invariant mass of the $Z^\star+\gamma_{\text{beamstrahlung}}$ system, which is larger than the mass of the $Z^\star$ alone. The seriousness of this effect will depend on the machine parameters, as well as on the chargino mass. For heavier charginos the cut on $m_{Z^\star}$ becomes stronger, so contamination from background events with hard collinear photons becomes less likely. Machine parameters for which the beamstrahlung photon typically carries less than 10% of the beam energy should not greatly distort $m_{Z^\star}$; our ability to make the $m_{Z^\star}$ cut and measure the threshold onset of $\gamma\tilde{\chi}_1^+\tilde{\chi}_1^-$ would not be significantly impaired.

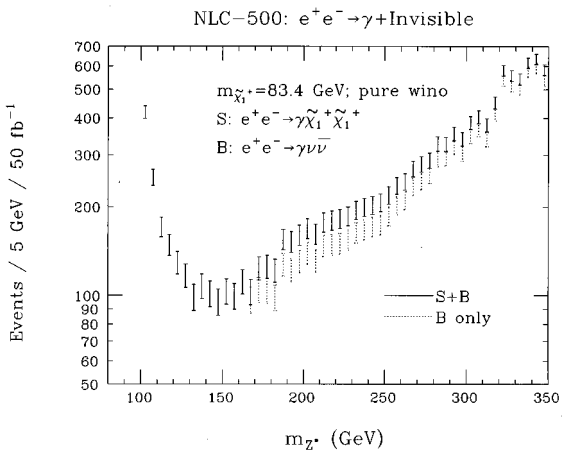

FIG. 12. For $e^+e^-\to\gamma+\not{E}_T$, we plot the the number of events per 5 GeV bin per $L=50$ fb^{-1} at NLC-500 as a function of $m_{Z\star}$. Solid error bars are for the sum of $\gamma\widetilde{\chi}_1^+\widetilde{\chi}_1^- + \gamma\nu\overline{\nu}$, while dotted error bars indicate expectations for $\gamma\nu\overline{\nu}$ alone. We have chosen a scenario with $m_{\widetilde{\chi}_1^\pm}=83.4$ GeV in which the $\widetilde{\chi}_1^\pm$ is pure wino. Photon cuts are as described in the text.

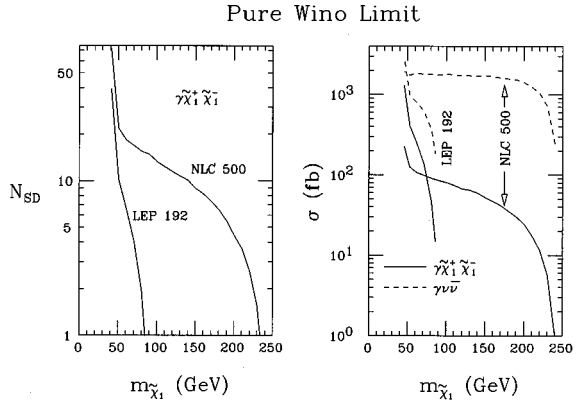

FIG. 13. We plot the statistical significance $N_{\rm SD}=S/\sqrt{B}$ for detecting $\gamma\widetilde{\chi}_1^+\widetilde{\chi}_1^-$ in the $\gamma+\not{E}_T$ channel as a function of $m_{\widetilde{\chi}_1^\pm}$. The background rate, B, is computed from $e^+e^-\to\gamma\nu\overline{\nu}$ by integrating over $m_{Z\star}\geq 2m_{\widetilde{\chi}_1^\pm}$. Results for LEP-192 (with $L=0.5$ fb^{-1}) and NLC-500 (with $L=50$ fb^{-1}) are displayed. Also shown are the $\gamma\widetilde{\chi}_1^+\widetilde{\chi}_1^-$ and $\gamma\nu\overline{\nu}$ cross sections themselves. We employ the cuts $p_T^\gamma\geq 10$ GeV and $10°\leq\theta_\gamma\leq 170°$. Results are for a chargino that is pure wino; slepton and sneutrino masses are assumed to be large.

signals with good overall statistical significance (in most cases $N_{\rm SD}$, defined below, $\gtrsim 5$ is adequate) one can plot events as a function of $m_{Z\star}$ and look for the threshold at $2m_{\widetilde{\chi}_1}$ at which the spectrum starts to exceed the expectations from $\gamma\nu\overline{\nu}$. This is illustrated for NLC-500 in Fig. 12, where we plot the number of events per 5 GeV bin as a function of $m_{Z\star}$ assuming $L=50$ fb^{-1}, comparing a $m_{\widetilde{\chi}_1}=83.4$ GeV signal with expectations for the $\gamma\nu\overline{\nu}$ background alone. Expected error bars are shown. We see that a determination of the threshold within about ± 10 to ± 15 GeV should prove possible in this case.

We define an overall statistical significance $N_{\rm SD}=S/\sqrt{B}$ for the signal by summing over all events with $m_{Z\star}>2m_{\widetilde{\chi}_1^\pm}$. Note, in particular, that this cut eliminates the Z-pole contribution to the $\gamma\nu\overline{\nu}$ background when $m_{\widetilde{\chi}_1^\pm}>m_Z/2$. The results for $N_{\rm SD}$ as a function of $m_{\widetilde{\chi}_1^\pm}$, as well as the $S=\gamma\widetilde{\chi}_1^+\widetilde{\chi}_1^-$ and $B=\gamma\nu\overline{\nu}$ cross sections (after integrating over $m_{Z\star}\geq 2m_{\widetilde{\chi}_1^\pm}$), are plotted in Fig. 13. For the particular example of Fig. 12 ($m_{\widetilde{\chi}_1^\pm}=83.4$ GeV, $\sqrt{s}=500$ GeV, and $L=50$ fb^{-1}), we find $S/\sqrt{B}\sim 15$. In practice, one can often do better (perhaps by 1σ to 2σ) than the nominal $N_{\rm SD}$ values plotted in Fig. 13 by zeroing in on those $m_{Z\star}$ bins with the largest deviations from $\gamma\nu\overline{\nu}$ expectations.

From the results of Fig. 13 we see that at NLC-500 (LEP-192) $N_{\rm SD}=5$ is achieved for $m_{\widetilde{\chi}_1^\pm}\lesssim 200$ GeV ($\lesssim 65$ GeV). Thus, one could not probe all the way to the $m_{\widetilde{\chi}_1^\pm}\sim\sqrt{s}/2$ kinematical limit, as would be possible in the $e^+e^-\to\widetilde{\chi}_1^+\widetilde{\chi}_1^-$ channel for conventional universal boundary conditions.

The situation is very different if one can detect the (soft) decay products or vertex tracks of the $\widetilde{\chi}_1^+\widetilde{\chi}_1^-$ in the $\gamma\widetilde{\chi}_1^+\widetilde{\chi}_1^-$ final state, since then $\gamma\nu\overline{\nu}$ production is no longer a background. The only background requiring discussion is that from $e^+e^-\to e^+e^-\gamma l^+l^-$, with two leptons disappearing down the beam pipe. This is a potential background to final states in which both the $\widetilde{\chi}_1^+$ and $\widetilde{\chi}_1^-$ decay leptonically. However, it will be very small. First, it will be greatly suppressed (although not entirely eliminated) by using the vetoing procedure outlined above. Second, it is $\mathcal{O}(\alpha^5)$ vs $\mathcal{O}(\alpha^3)$ for the signal. Third, the enhancement deriving from singular t-channel photon exchange is only operative and escapes the veto if the energetic e^+e^- both disappear down the beam pipe, implying that the observed soft leptons (i.e., the $\ell^+\ell^-$ pair) must be of the same type; the background due to this configuration could thus be eliminated by focusing on the soft $e^+\mu^-$ and μ^+e^- pairs that are just as probable as $\mu^+\mu^-$ or e^+e^- pairs in $\widetilde{\chi}_1^+\widetilde{\chi}_1^-$ decays (assuming that we can distinguish a muon from an electron at low energy). Only $\ell^+\ell^-=\tau^+\tau^-$ could yield $e\mu$ final states. Thus, we believe that backgrounds to $\gamma\widetilde{\chi}_1^+\widetilde{\chi}_1^-$ production are negligible when the soft $\widetilde{\chi}_1^+\widetilde{\chi}_1^-$ decay products are visible.

In the absence of significant background, the observability of $e^+e^-\to\gamma\widetilde{\chi}_1^+\widetilde{\chi}_1^-$ followed by detection of the soft decay products or short tracks of the $\widetilde{\chi}_1^+\widetilde{\chi}_1^-$ depends entirely on event rate. The latter is simply given by the luminosity times the cross section plotted in Fig. 13. Assuming 50 (background free) events are required, we could detect $\gamma\widetilde{\chi}_1^+\widetilde{\chi}_1^-$ at NLC-500 (LEP-192) all the way up to 240 GeV (75 GeV) for $L=50$ fb^{-1} (0.5 fb^{-1}). The increase in discovery range compared to the case where the $\widetilde{\chi}_1^+\widetilde{\chi}_1^-$ are invisible to the detector is especially marked at the NLC, with the mass reach improving almost to the $\sqrt{s}/2$ kinematical limit.

D. SUSY discovery at hadron colliders

As noted earlier, detection of a signal from supersymmetric particle production at a hadron collider need not be straightforward in the O-II model scenario. Since the squarks and sleptons are necessarily very heavy in the O-II model (unless $|\delta_{\rm GS}|$ is very large), gluino-pair and electroweak-gaugino-pair production would appear to provide the greatest potential for SUSY discovery. While this is certainly the case at the Tevatron, gluino-squark and squark-squark pair production at the LHC would be possible. We will comment on these SUSY signals later.

First, we focus on electroweak-gaugino-pair and gluino-pair production. The primary channel for detecting the former is normally the 3ℓ channel deriving from $\tilde{\chi}_1^{\pm}\tilde{\chi}_2^0 \to \ell^{\pm}\ell^{+}\ell^{-}\not{E}_T X$. If $\Delta m_{\tilde{\chi}_1}$ is small (small $|\delta_{\rm GS}|$) the ℓ from $\tilde{\chi}_1^{\pm} \to \ell^{\pm}\nu\tilde{\chi}_1^0$ decay is so soft that the 3ℓ signal is negligible. The two primary modes for detecting $\tilde{g}\tilde{g}$ pair production are the jets$+\not{E}_T$ channel and the like-sign dilepton, $\ell^{\pm}\ell^{\pm}+$jets$+\not{E}_T$ signal. The like-sign dilepton signal (from $\tilde{g}\tilde{g} \to \tilde{\chi}_1^{\pm}\tilde{\chi}_1^{\pm}X \to \ell^{\pm}\ell^{\pm}\not{E}_T X$) will be negligible if $\Delta m_{\tilde{\chi}_1}$ is small because of the softness of the leptons. To the extent that it is not observable, it will add to the jets$+\not{E}_T$ signal (which is defined by events having no observable hard lepton).

Depending upon the model parameters, the jets$+\not{E}_T$ signal for $\tilde{g}\tilde{g}$ production may also be difficult to isolate from background. If $-\delta_{\rm GS}$ is such that $m_{\tilde{g}} \sim m_{\tilde{\chi}_1}$, the jets from $\tilde{g}$ decay are softer than for the universal boundary condition models which have $m_{\tilde{g}} \sim 3m_{\tilde{\chi}_1^{\pm}} \sim 6m_{\tilde{\chi}_1^0}$. This is illustrated in Fig. 14. There, the $\not{E}_T$ spectra for the most energetic three jets and for $\not{E}_T$ as predicted for universal boundary conditions and in the $\delta_{\rm GS}=-5$ O-II model are compared at the Tevatron. (This figure includes the effects of jet energy smearing.) The jets are much harder in the former case due to the large $m_{\tilde{g}} - m_{\tilde{\chi}_1^{\pm}} \sim 200$ GeV and $m_{\tilde{g}} - m_{\tilde{\chi}_1^0} \sim 250$ GeV mass differences as compared to $m_{\tilde{g}} - m_{\tilde{\chi}_1} \sim 76$ GeV for the O-II model. Correspondingly, $\not{E}_T$ is somewhat larger on average in the O-II model. In the following, we determine the portion of $\delta_{\rm GS} - m_{\tilde{g}}$ parameter space (equivalently $\delta_{\rm GS} - m_0$ parameter space, see Fig. 5) for which the jets$+\not{E}_T$ signal will be visible at the Tevatron and TeV*.

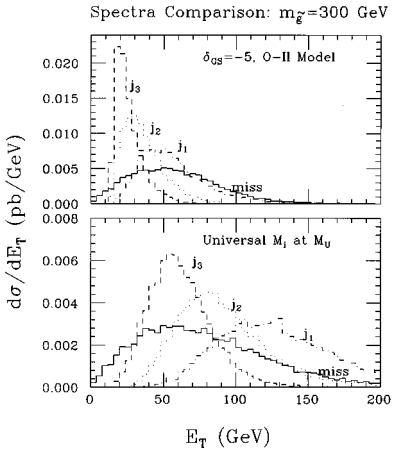

FIG. 14. Spectra, $d\sigma/dE_T$, vs E_T for the three most energetic jets (labeled j_1, j_2, j_3 in order of decreasing E_T) and the missing energy. The spectra for the universal boundary condition model and the O-II model with $\delta_{\rm GS}=-5$ are compared for $m_{\tilde{g}}=300$ GeV, $\tan\beta=2$ at the Tevatron. Jet-energy smearing effects are included.

1. The jets$+\not{E}_T$ SUSY signal

At the Tevatron or TeV*, we consider both D0 [13] and CDF [14] cuts. These are summarized below.[6]

D0 cuts: There are no isolated leptons with $E_T > 15$ GeV, where isolation is defined by requiring that additional E_T within $\Delta R \leq 0.3$ of the lepton be <5 GeV. $\not{E}_T > 75$ GeV. There are n(jets)≥ 3 jets having $|\eta_{\rm jet}| < 3.5$ and $E_T > 25$ GeV, using a coalescence cone size of $\Delta R = 0.5$. These are ordered according to decreasing E_T and labeled by $k=1,2,3$. The azimuthal separations of the $k=1,2,3$ jets from the $\not{E}_T$ vector, $\delta\phi_k \equiv \Delta\phi(\not{E}_T, jk)$, are required to satisfy $0.1 < \delta\phi_k < \pi - 0.1$. It is further required that $\sqrt{(\delta\phi_1 - \pi)^2 + \delta\phi_2^2} > 0.5$.

CDF cuts: There are no leptons with $E_T > 10$ GeV. $\not{E}_T > 60$ GeV. There are n(jets)≥ 3 jets having $|\eta_{\rm jet}| < 2$ and $E_T > 15$ GeV, using a coalescence cone size of $\Delta R = 0.5$. Azimuthal separation requirements are the following: $\Delta\phi(\not{E}_T, j_1) < 160°$; and $\Delta\phi(\not{E}_T, j(E_T > 20\ \text{GeV})) > 30°$. These are designed, in particular, to reduce QCD jet mismeasurement.

We note that the lepton cut causes no signal loss when the $\tilde{\chi}_1^{\pm}$ decay leptons are very soft. (In comparison, in the universal boundary condition scenarios signal events sometimes have isolated leptons.)

Our procedure will be to compute the signal cross section, σ_S, at the Tevatron as a function of $\delta_{\rm GS}$ and $m_{\tilde{g}}$ after imposing the two different sets of cuts listed above. For the background rates we take the D0 and Collider Detector at Fermilab (CDF) cross sections as computed in Refs. [13,14] for the above cuts, respectively. For D0 cuts, the background cross section is taken from Table 1 of Ref. [13] to be 16.7 events for $L = 7.1\ \text{pb}^{-1}$, corresponding to a cross section of $\sigma_B = 2.35$ pb. For CDF cuts, Ref. [14] quotes a background rate of 28.7 events for $L = 19\ \text{pb}^{-1}$, corresponding to $\sigma_B = 1.51$ pb. For a given luminosity, we compute the background and signal rates as $S = L\sigma_S$ and $B = L\sigma_B$, respectively. Both the D0 and CDF background computations include full hadronic energy smearing and the like, so that some of the background rate may come from fake $\not{E}_T$. We also include the effects of hadronic energy smearing in the signal rate computation.

Before presenting an overall summary graph, it is useful to explicitly demonstrate the impact of the softness of the jets when near the $m_{\tilde{g}} \sim m_{\tilde{\chi}_1}$ boundary. In Fig. 15 the cross sections at the Tevatron, after imposing D0 cuts, are displayed in two cases: increasing $m_{\tilde{g}}$ by increasing m_0 while holding fixed $\delta_{\rm GS}=-4.2$ (i.e., near the degeneracy boundary); and increasing $m_{\tilde{g}}$ by increasing $-\delta_{\rm GS}$ while holding fixed $m_0 = 1$ TeV (i.e., moving rapidly away from the degeneracy boundary).

The rapid decline of the cross section in the former case, as compared to the latter, is apparent. The Tevatron will not be able to detect $\tilde{g}\tilde{g}$ production out to as large an $m_{\tilde{g}}$ along the degeneracy boundary as away from it.

In Fig. 16 we show the $\delta_{\rm GS} - m_{\tilde{g}}$ parameter space regions for which the jets$+\not{E}_T$ signal should have been observed or will be observable for various different integrated luminosities, when the D0 or CDF cuts outlined above are employed. Observability is defined by $S/\sqrt{B} \geq 5$ *and* $S/B \geq 0.2$, where S

[6]We presume that the cuts of Ref. [13] that are designed to eliminate jets formed around noisy calorimeter cells and jets induced by particles from the main ring accelerator do not significantly reduce the signal cross section.

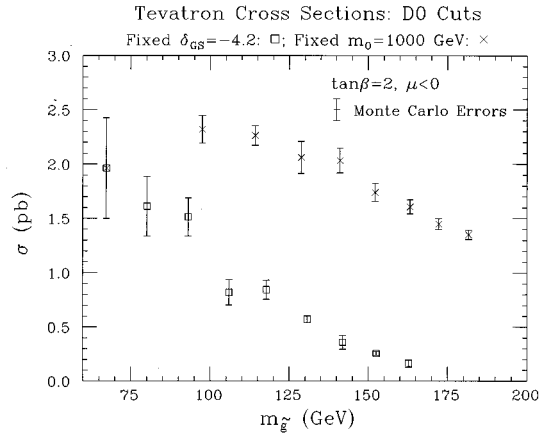

FIG. 15. Cross section after D0 cuts at the Tevatron as a function of $m_{\tilde{g}}$ for (i) fixed $\delta_{GS}=-4.2$ along the $m_{\tilde{g}}\sim m_{\tilde{\chi}_1}$ [see Eq. (8)] boundary—plotted points correspond to $m_0=1$, 1.2, 1.4, 1.6, 1.8, 2.2, 2.4, and 2.6 TeV; (ii) fixed $m_0=1$ TeV with increasing $-\delta_{GS}$—plotted points are at $-\delta_{GS}=4.2$, 5, 5.5, 6, 6.5, 7, 7.5, 8, and 8.5. We have taken tan$\beta=2$ and $\mu<0$.

and B are the numbers of signal and background events, respectively, for a given luminosity. The $S/B\geq 0.2$ requirement above is needed due to the rather featureless nature of the signal which makes it difficult to distinguish from the background using anything other than the integrated cross section level. It is the limiting factor in the maximum $m_{\tilde{g}}$ value that can be probed at high luminosity. The four different sets of symbols indicate the following.

Pluses indicate parameter space points that can be excluded by analysis of roughly $L=8$ pb^{-1} of data from Run-Ia. This is the amount of data for which D0 has published an analysis and claimed to see no signal.

Diamonds (together with pluses) indicate parameter space points excluded for $L=19$ pb^{-1} of Run-Ia data. This is the amount of data analyzed and published by CDF without observing a signal.

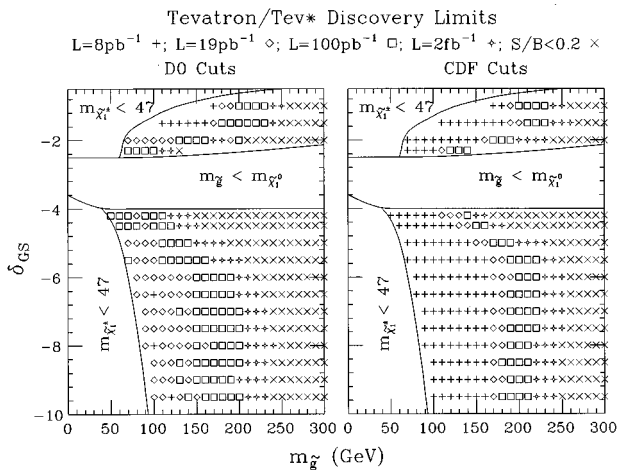

FIG. 16. O-II model regions of the $\delta_{GS}-m_{\tilde{g}}$ parameter space for which $\tilde{g}\tilde{g}$ production can be detected at the Tevatron/TeV* in the jets+$\not{E}_T$ channel for various different luminosities, using the cuts described in the text. Open points are excluded, as indicated, either by the LEP constraint of $m_{\tilde{\chi}_1^\pm}\geq 47$ GeV or by $m_{\tilde{g}}<m_{\tilde{\chi}_1^0}$. We have taken tan$\beta=2$ and $\mu<0$.

Squares indicate additional points that will be excluded for accumulated luminosity of $L=100$ pb^{-1}, i.e., if no signal is observed after the full Run-Ia+Run-Ib data are analyzed. Such analyses should be available in the near future.

Next come the points indicated by a small starlike symbol that can be excluded for $L=2$ fb^{-1}, i.e., after one year of running at the projected main injector luminosity.

For the points indicated by an ×, $S/B<0.2$ and no amount of luminosity suffices. Systematics would have to be controlled at the $\lesssim$10% level to access this region.

Three distinct regions of δ_{GS} are apparent in Fig. 16.

(1) When $|\delta_{GS}|$ is large the upper limits on $m_{\tilde{g}}$ for which the signal can be detected become independent of δ_{GS} and asymptote to those for which $\tilde{g}\tilde{g}$ pair production could be observed in the universal boundary condition scenario for a given set of cuts (taking squarks to be much heavier than the $\tilde{g}$). This asymptote is reached already for $-\delta_{GS}\gtrsim 10$ since for such values $m_{\tilde{g}}/m_{\tilde{\chi}_1^\pm}\sim 3$ (as for universal boundary conditions), despite the fact that $m_{\tilde{\chi}_1^\pm}/m_{\tilde{\chi}_1^0}$ does not reach the universal boundary condition result of ~ 2 even by $\delta_{GS}=-20$.

(2) When $|\delta_{GS}|$ is small, the ratio $m_{\tilde{g}}/m_{\tilde{\chi}_1^\pm}$ exceeds the value ~ 3 typical of the universal boundary condition scenario, and even higher values of $m_{\tilde{g}}$ can be probed due to the increased energy of the jets from $\tilde{g}$ decay, coupled with the fact that there is no loss of jets+$\not{E}_T$ signal from the restriction against isolated leptons.

(3) For δ_{GS} such that $m_{\tilde{g}}-m_{\tilde{\chi}_1^\pm}$ and $m_{\tilde{g}}-m_{\tilde{\chi}_1^0}$ are small, the reach in $m_{\tilde{g}}$ is reduced, although perhaps less severely than naively anticipated. The reason for this latter is that even for small mass difference, it is still possible to get energetic jets from initial and final state radiation rather than from the $\tilde{g}$ decay. For most events at least one of the three most energetic jets is radiative in nature when $m_{\tilde{g}}\sim m_{\tilde{\chi}_1}$, whereas for the universal boundary condition scenario the most energetic jets are almost always from the $\tilde{g}$ decays.

In Table I we give the maximum $m_{\tilde{g}}$ values that can be probed in the jets+$\not{E}_T$ channel, using the D0 or CDF jet cuts delineated earlier, at $\delta_{GS}=-1$, $\delta_{GS}=-4.5$ (near the $m_{\tilde{g}}\sim m_{\tilde{\chi}_1^\pm}$ boundary), and $\delta_{GS}=-10$. Notice that there is no gain in discovery reach in going from $L=2$ fb^{-1} (typical of the main injector) to TeV* luminosity of $L=25$ fb^{-1}. This is due to the fact that the maximum $m_{\tilde{g}}$ values that can be probed at $L=2$ fb^{-1} are determined by S/B falling below the minimum value of 0.2. For both the D0 and CDF cuts B is relatively large. If systematic uncertainties in the predicted level of the jets+$\not{E}_T$ signal due to theoretical and experimental uncertainties can be reduced below the $\sim$10% level, higher values of $m_{\tilde{g}}$ could be probed.

The most striking difference between the D0 and CDF cuts is the much greater sensitivity of the softer CDF cuts to parameter choices for which $m_{\tilde{g}}\sim m_{\tilde{\chi}_1^\pm}\sim m_{\tilde{\chi}_1^0}$. The reason for this striking difference is that the D0 cuts include a fairly stiff minimum $E_T=25$ GeV requirement for the third jet. As shown in Fig. 14, for scenarios with a small $m_{\tilde{g}}-m_{\tilde{\chi}_1}$ mass splitting this will eliminate a substantial fraction of the signal events. Weakening this cut, as in the CDF procedure, increases the signal rate, and apparently does so without increasing the background rate (perhaps because stronger rapidity cuts are imposed on the jets in the CDF procedure). It

TABLE I. Maximum $m_{\tilde{g}}$ values that can be probed using D0 and CDF cuts (see text) in the jets+$\not{E}_T$ final state for different integrated luminosities, L, at the Tevatron and TeV* at $\delta_{GS}=-10$, $\delta_{GS}=-1$, and $\delta_{GS}=-4.5$. Observability is defined by $S/\sqrt{B}\geq 5$ and $S/B\geq 0.2$. Also given are the maximum $m_{\tilde{g}}$ values for which $\tilde{g}\tilde{g}$ production can be observed in the (universal boundary condition) limit of very large $|\delta_{GS}|$ using the stronger cuts of Ref. [15]. The results of this table are for $\tan\beta=2$ and $\mu<0$.

Cuts	$L=$	8 pb^{-1}	19 pb^{-1}	100 pb^{-1}	2 fb^{-1}	25 fb^{-1}
	$\delta_{GS}=-1$	170 GeV	200 GeV	230 GeV	250 GeV	250 GeV
D0	$\delta_{GS}=-4.5$	-	80 GeV	110 GeV	150 GeV	150 GeV
	$\delta_{GS}=-10$	-	140 GeV	200 GeV	200 GeV	200 GeV
	$\delta_{GS}=-1$	180 GeV	190 GeV	230 GeV	250 GeV	250 GeV
CDF	$\delta_{GS}=-4.5$	100 GeV	130 GeV	140 GeV	160 GeV	160 GeV
	$\delta_{GS}=-10$	150 GeV	170 GeV	210 GeV	240 GeV	240 GeV
Strong	$\delta_{GS}\to-\infty$	$m_{\tilde{g}}$ excluded by $m_{\tilde{\chi}_1^\pm}\leq 47$ GeV			250 GeV	300 GeV

will be important for the CDF and D0 Collaborations to determine if there are still more optimal cuts for scenarios with small mass splitting. We note that the greater sensitivity of CDF cuts persists up to $|\delta_{GS}|\sim 10$, even though $m_{\tilde{g}}-m_{\tilde{\chi}_1^\pm}$ approaches values typical of universal boundary conditions. In contrast, the difference between D0 and CDF cuts disappears at small $|\delta_{GS}|$ where $m_{\tilde{g}}-m_{\tilde{\chi}_1^\pm}$ is even larger than predicted for universal boundary conditions.

It is important to note that the jet cuts employed here are no longer optimal in the universal boundary condition limit (roughly $-\delta_{GS}\gtrsim 10$–20) when $L>2$ fb^{-1} and $m_{\tilde{g}}$ is large. It is better to strengthen the cuts. This is due to the fact that stronger cuts will reduce the background rate B while leaving good efficiency for the signal if $m_{\tilde{g}}$ is large and there is substantial mass splitting between the $\tilde{g}$ and the $\tilde{\chi}_1^\pm$ and $\tilde{\chi}_1^0$. This leads to $S/B>0.2$ at high $m_{\tilde{g}}$. The stronger (more optimal) cuts employed at high L are discussed in Ref. [15]. For the jets+$\not{E}_T$ channel they are: $\not{E}_T>40$ GeV; $n(\text{jets})\geq 2$ jets having $|\eta_{\text{jet}}|<3$ and $E_T(\text{jet})>15$ GeV; transverse sphericity $S_T\geq 0.2$; $\Delta\phi(\not{E}_T, j(E_T>15\text{ GeV}))>30°$; and $E_T(j_1)$, $E_T(j_2)\geq E_T^c$ and $\not{E}_T\geq E_T^c$, with E_T^c optimized for given L, $m_{\tilde{g}}$ and other and parameter choices.

To give an example, the $m_{\tilde{g}}=300$ GeV detection limit in Table I for universal boundary conditions is attained using $E_T^c=100$ GeV. It is also possible that the stronger cuts would allow us to probe to higher $m_{\tilde{g}}$ values at small $|\delta_{GS}|$ than accessible using the weaker D0 and CDF jet cuts (see Fig. 16). This is because $m_{\tilde{g}}/m_{\tilde{\chi}_1^\pm}\sim m_{\tilde{g}}/m_{\tilde{\chi}_1^0}$ is large and the jets would be energetic. However, we have not performed a detailed analysis.

The limitations on the $m_{\tilde{g}}$ discovery reach in the case of $m_{\tilde{g}}$ near $m_{\tilde{\chi}_1}$ are not quite as much of a concern as one might first suppose. This is because the $m_0\lesssim 2$ TeV naturalness requirement imposes an upper bound of $m_{\tilde{g}}\gtrsim 140$ GeV in the $m_{\tilde{g}}\sim m_{\tilde{\chi}_1^\pm}$ boundary region, see Fig. 5. From Fig. 16 and Table I we see that this value of $m_{\tilde{g}}$ can be probed at $\delta_{GS}=-4.5$ with $L=100$ pb^{-1}, provided CDF-like cuts are employed. In contrast, for $\delta_{GS}=-10$, from Fig. 5 $m_{\tilde{g}}\gtrsim 350$ GeV if $m_0=2$ TeV and $\tilde{g}\tilde{g}$ pair production would not be observable even at TeV*.

Turning now to the LHC, the standard cuts employed there in the universal boundary condition model are [16]: there are no isolated leptons with $E_T>20$ GeV, where isolation is defined by requiring that additional E_T within $\Delta R\leq 0.3$ of the lepton be <5 GeV; transverse sphericity of $S_T>0.2$; $\not{E}_T>500$ GeV; $n(\text{jets})\geq 2$ having $|\eta_{\text{jet}}|<3$ and $E_T>100$ GeV using coalescence within $\Delta R\leq 0.7$; $30°\leq\Delta\phi(\not{E}_T,\text{jet})<90°$ for the jet which is closest to the $\not{E}_T$ vector; and $E_T(j_1,j_2)\geq 500$ GeV, where the jets are ordered by E_T.

For these cuts, $\tilde{g}\tilde{g}$ pair production in the O-II model is not observable in any part of the $|\delta_{GS}|<10$ portion of parameter space appearing in Fig. 16. Hopefully, this will be cured by weakening the jet cuts. Optimization of the cuts and assessment of the signals is underway and will be presented elsewhere.

2. Leptonic signals for $\tilde{g}\tilde{g}$ production

We have already remarked that if $m_{\tilde{\chi}_1^\pm}\sim m_{\tilde{\chi}_1^0}$, then it will be far more difficult to extract a like-sign dilepton signal for $\tilde{g}\tilde{g}$ production than is the case for universal boundary conditions. The leptons from the $\tilde{\chi}_1^\pm$ decays will be much softer when $\Delta m_{\tilde{\chi}_1}$ is small. A detailed study will be required to determine if any signal survives. We believe it is unlikely that the dilepton signal can achieve as much discovery reach as the jets+$\not{E}_T$ signal.

When $m_{\tilde{g}}$ is close to $m_{\tilde{\chi}_1}$, there are no other sources of leptons than those from the $\tilde{\chi}_1^\pm$'s that are present in the $\tilde{g}$ decays. As $m_{\tilde{g}}$ becomes larger than $m_{\tilde{\chi}_1}$, not only does the jets+$\not{E}_T$ signal become increasingly strong, but also additional leptonic signals for $\tilde{g}\tilde{g}$ production emerge deriving from $\tilde{g}\to$jets+$\tilde{\chi}_2^0$ decay followed by $\tilde{\chi}_2^0\to\ell^+\ell^-\tilde{\chi}_1^0$, dominated by the on-pole $Z\tilde{\chi}_1^0$ final state when kinematically allowed. A detailed study is required to determine if the resulting signal for $\tilde{g}\tilde{g}$ production is competitive with the jets+$\not{E}_T$ signal. Ultimately, in the very large $|\delta_{GS}|$ universal boundary condition limit, the presence of the many cascade decays by which $\tilde{g}\tilde{g}$ production leads to leptons results in a $\ell^\pm$+jets+$\not{E}_T$ signal that is stronger than the jets+$\not{E}_T$ signal at the LHC [16].

3. The trilepton signal

We have also performed explicit simulations for the trilepton signal at the Tevatron. A summary of current CDF and D0 cuts and results appears in Ref. [17]. In our analysis we consider two sets of cuts. The first set of cuts is that employed by CDF in analyzing their $L=100$ pb^{-1} data set: $|\eta(\ell_{1,2,3})|\leq 2.5$; $E_T(\ell_1)>11$ GeV, $E_T(\ell_{2,3})>4$ GeV; $\not{E}_T>15$

GeV; $n(\text{jets})=0$ for jets with $E_T>15$ GeV; events with e^+e^- or $\mu^+\mu^-$ pairs with mass $\sim m_Z$ are vetoed.

The second set of cuts [15] was designed to detect 3ℓ events at luminosities $\gtrsim 1$ fb^{-1} (main injector and TeV*) in the universal boundary condition scenario. The latter cuts (which we call the ''strong'' cuts) are $|\eta(\ell_{1,2,3})|\leqslant 2.5$; $E_T(\ell_{1,2,3})\geqslant 20,15,10$ GeV, respectively; $\not{E}_T\geqslant 25$ GeV; $n(\text{jets})=0$ for jets with $E_T>15$ GeV; events with e^+e^- or $\mu^+\mu^-$ pairs with mass $\sim m_Z$ are vetoed.

For the CDF cuts the background was taken from Ref. [17] as 0.4 events for $L=100$ pb^{-1}, corresponding to a cross section of $\sigma_B=4$ fb. For other luminosities the number of background events was computed as $L\sigma_B$. For the second set of cuts, the background was explicitly computed using ISAJET, summing over all important reactions. For both sets of cuts, the 3ℓ signal is deemed observable if there are at least 5 events, $S/\sqrt{B}\geqslant 5$ and $S/B\geqslant 0.2$.

For either set of cuts, the 3ℓ signature is unobservable for any luminosity unless $\delta_{\rm GS}$ is well above the region where $\Delta m_{\tilde{\chi}_1}$ is small. At $\delta_{\rm GS}=-9$, the 3ℓ remains unobservable for both sets of cuts at $L=100$ fb^{-1}. For the CDF (strong) cuts, a 3ℓ signal becomes observable at $\delta_{\rm GS}=-9$ for $m_{\tilde{g}}$ values up to 160 GeV (100 GeV) with $L=2$ fb^{-1} and up 210 GeV (160 GeV) with $L=25$ fb^{-1}. The fact that the strong cuts do not allow as much sensitivity to the 3ℓ signal as do the weaker CDF cuts is obviously a result of the fact that the leptons remain soft (as compared to universal boundary condition expectations) in the O-II model out to quite large $|\delta_{\rm GS}|$.

4. Gluino-squark and squark-squark pair production

Production of $\tilde{g}\tilde{q}$ and $\tilde{q}\tilde{q}$ pairs will occur at a significant rate at the CERN Large Hadron Collider (LHC), even for squark masses of 1 TeV or more. These pair production processes would be followed by $\tilde{q}\to\tilde{g}q$ decay, leading to final states comprised of $\tilde{g}\tilde{g}q$ and $\tilde{g}\tilde{g}qq$, respectively. The $\tilde{g}$'s would then decay as we have described. In particular, it is very possible that most of the energy of the $\tilde{g}$ will go into the $\tilde{\chi}_1^0$. Thus, even though the $\tilde{g}$'s from the $\tilde{q}$ decays would be energetic, the visible jet energy component of the decay need not be large. Further, it will tend to be aligned with the missing energy component due to the large momentum of the $\tilde{g}$ coming from decay of a very heavy $\tilde{q}$.

Thus, $\tilde{g}\tilde{q}$ production will lead to a final state with a very energetic quark and large missing energy in the opposite direction. Backgrounds to this configuration need to be studied to determine if the signal for such events can be found. (An obvious background is $Z+g$ production in which the Z decays invisibly.) We have not attempted this study here. The $\tilde{q}\tilde{q}\to qq\tilde{g}\tilde{g}\to qq\not{E}_T+$soft signal for SUSY is not very different than that already considered (see, e.g., Ref. [16]) for $\tilde{q}\tilde{q}$ production in the case of universal boundary conditions. The final state would consist of two highly energetic jets along with large $\not{E}_T$, all in different directions; backgrounds will be small, and detection of the signal should be straightforward for $m_{\tilde{g}}\lesssim 1.5$–$2$ GeV at the LHC [16,18–20]. For both $\tilde{g}\tilde{q}$ and $\tilde{q}\tilde{q}$ production, it could be that stop and sbottom squarks would be easiest to trigger on due to the fact that the final states would contain two t's or two b's, respectively. (Note that in $\tilde{g}\tilde{q}$ production with $\tilde{q}=\tilde{t}$ or $\tilde{b}$, there must be an associated t or b, respectively.) In the case of $\tilde{g}\tilde{q}$ ($\tilde{q}\tilde{q}$) production, with $\tilde{q}=\tilde{t}$ or $\tilde{b}$, one (both) of the t's or b's would be very energetic. Vertex b tagging could be used to isolate the relevant events. A close examination of these signals is warranted.

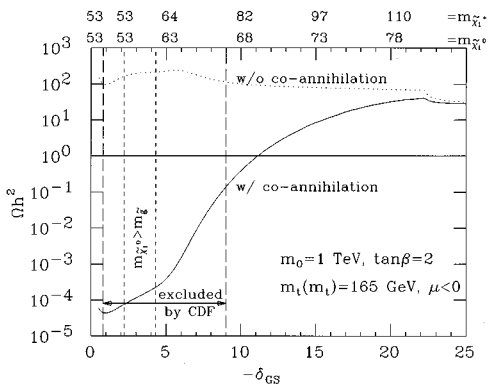

FIG. 17. We plot the relic density Ωh^2 as a function of $\delta_{\rm GS}$ with and without including $\tilde{\chi}_1^\pm\tilde{\chi}_1^0$ coannihilation. We take $m_0=1$ TeV, $\tan\beta=2$, $m_t(m_t)=165$ GeV, and $\mu<0$. The region defined by the vertical short-dashed lines is disallowed because the $\tilde{g}$ would be the LSP. The region defined by the vertical long-dashed lines is excluded by the failure of the CDF Collaboration to detect a jets+$\not{E}_T$ signal from $\tilde{g}\tilde{g}$ production for $L=19$ pb^{-1} of data.

E. Implications for cosmology

One of the attractive features of supersymmetry is that the LSP could provide a natural source for the dark matter that appears to be required by galactic rotational data (requiring $\Omega h^2>0.025$) and that would be needed for closure of the Universe ($\Omega=1$); further, $\Omega h^2\lesssim 1$ is required in order that the universe be at least 10 billion years old. [Here, Ω is the present LSP mass density in units of the critical or closure density, and h is the Hubble constant in units 100 km/(s Mpc).] The $m_{\tilde{\chi}_1^+}\simeq m_{\tilde{\chi}_1^0}$ degeneracy and SU(2)-gaugino nature of the $\tilde{\chi}_1^0$ predicted in the $\sin\theta\to 0$ O-II model when $|\delta_{\rm GS}|$ is not large leads to a picture that differs substantially from that found for universal boundary conditions. The two key differences are easily summarized.

(1) For moderate to small $|\delta_{\rm GS}|$ in the O-II model, $\tilde{\chi}_1^0\tilde{\chi}_1^0$ annihilation is quite small because the $\tilde{\chi}_1^0$ is usually almost pure SU(2) gaugino and its couplings to the light Higgs (h^0) and the Z are weak (they require a Higgsino component) and because the sfermions are typically very heavy [as discussed with regard to Eqs. (6) and (7), and following].

(2) The near degeneracy $m_{\tilde{\chi}_1^\pm}\simeq m_{\tilde{\chi}_1^0}$ implies (as noted several years ago in Ref. [7]) similar densities (due to very similar Boltzmann factors) for the $\tilde{\chi}_1^\pm$ and $\tilde{\chi}_1^0$ at the time of freeze-out, so that coannihilation between the LSP and the chargino becomes very important and can greatly reduce the expected relic density.

The computation of the relic density is sketched in Appendix B. As well as the $\tilde{\chi}_1^\pm\tilde{\chi}_1^0\to ff$ co-annihilation channel considered in [7], we also included the $\tilde{\chi}_1^\pm\tilde{\chi}_1^0\to W^\pm\gamma$ channel (a few percent effect). To illustrate the importance of coannihilation, we have plotted Ωh^2, before and after including coannihilation, as a function of $\delta_{\rm GS}$ (for $m_0=1$ TeV, $\tan\beta=2$, and $\mu<0$) in Fig. 17. From this figure, we observe that without coannihilation Ωh^2 is at least 10, and, at smaller

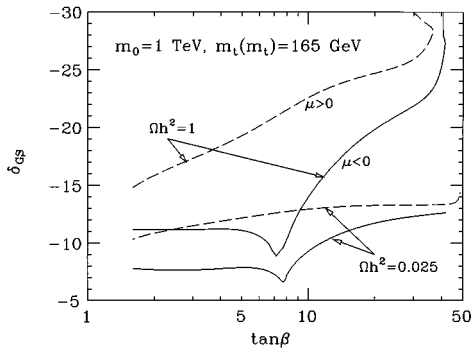

FIG. 18. Contours of constant $\Omega h^2=0.025$ and $\Omega h^2=1$ in $\tan\beta-\delta_{\rm GS}$ parameter space at $m_0=1$ TeV, for $\mu<0$ and $\mu>0$.

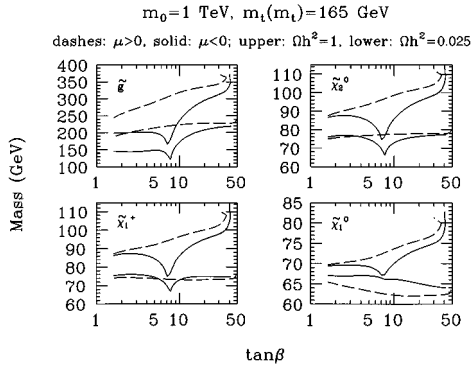

FIG. 19. Contours of constant $\Omega h^2=0.025$ and $\Omega h^2=1$ in the $\tan\beta-m_{\tilde g}, m_{\tilde\chi_1^\pm}, m_{\tilde\chi_1^0}, m_{\tilde\chi_2^0}$ parameter spaces at $m_0=1$ TeV, for $\mu<0$ and $\mu>0$.

$|\delta_{\rm GS}|$, as large as 100, i.e., drastically inconsistent with the fact that the Universe is still expanding. After including coannihilation, we see that $\Omega h^2<1$ for $|\delta_{\rm GS}|\lesssim 10$. Indeed, extremely small Ωh^2 values, $\lesssim 10^{-4}$, are possible for $|\delta_{\rm GS}|\lesssim 6$ where $\Delta m_{\tilde\chi_1}$ becomes small. As $|\delta_{\rm GS}|$ increases above this, coannihilation becomes ineffective when $\Delta m_{\tilde\chi_1}/m_{\tilde\chi_1^0}$ exceeds a few percent.

For the choice of parameters of Fig. 17, $\Omega h^2<1$ requires $m_{\tilde\chi_1^\pm}\lesssim 88$ GeV; direct detection of $\tilde\chi_1^+\tilde\chi_1^-$ production at LEP-II will be possible only for the portion of this range for which $\Delta m_{\tilde\chi_1}$ exceeds 5–10 GeV, i.e., roughly for $|\delta_{\rm GS}|\gtrsim 7$, see Fig. 4, corresponding to $m_{\tilde\chi_1^\pm}\gtrsim 70$ GeV. (This is precisely the range for which $\Omega h^2\gtrsim 0.025$, and the $\tilde\chi_1^0$ of the model could be the dark matter of the Universe.) For $m_{\tilde\chi_1^\pm}\lesssim 70$ GeV, it will become necessary to employ the $\gamma\tilde\chi_1^+\tilde\chi_1^-$ mode, see Fig. 13. The region of parameter space currently eliminated by the failure to observe $\tilde g\tilde g$ production at the Tevatron employing the published CDF analysis of $L\sim 19$ pb^{-1} of data is obtained by correlating $m_{\tilde g}$ and $\delta_{\rm GS}$ locations in Fig. 17 with the CDF excluded regions in Fig. 16; it is roughly $0.8\lesssim -\delta_{\rm GS}\lesssim 9$, as indicated in Fig. 17. (Because of stronger jet cuts and the smaller amount, $L=8$ pb^{-1}, of analyzed data, the currently published D0 analysis only excludes $1\lesssim -\delta_{\rm GS}\lesssim 1.6$.) For all but the $|\delta_{\rm GS}|<0.6$ portion of the $-\delta_{\rm GS}\lesssim 12$ range, $m_{\tilde g}$ is such that $\tilde g\tilde g$ production at the Tevatron could be detected using the CDF cuts and analysis procedures outlined in the preceding section applied to $L=100$ pb^{-1} of data, see Fig. 16. Thus, for the choices $\tan\beta=2$ and $m_0=1$ TeV, it is only for very small $|\delta_{\rm GS}|$ that the model can be consistent with an expanding universe if no signal for $\tilde g\tilde g$ production is found after analyzing Run-Ia+Run-Ib Tevatron data using the CDF procedures employed for Fig. 16. However, to repeat, small values of $|\delta_{\rm GS}|$ will not yield $\Omega h^2\gtrsim 0.025$.

The range of $\delta_{\rm GS}$ for which $0.025\lesssim\Omega h^2\lesssim 1$, especially the largest allowed $|\delta_{\rm GS}|$ value, typically increases with increasing $\tan\beta$. The regions with $0.025\lesssim\Omega h^2\lesssim 1$ are plotted in the $\delta_{\rm GS}$-$\tan\beta$ parameter space plane for $m_0=1$ TeV and both signs of μ in Fig. 18. Typically, only a narrow range of $\delta_{\rm GS}$ values satisfies both criteria unless $\tan\beta$ is very large. The lower bound on $-\delta_{\rm GS}$, set by requiring $\Omega h^2\gtrsim 0.025$ would not be present if some other explanation for dark matter is assumed to exist. Indeed, for the preferred model values of $\delta_{\rm GS}=-4,-5$ an alternative source of dark matter would be necessary.

To further delineate the consistency of existing and near future experimental data with the constraints on Ωh^2, it is illuminating to plot the $\Omega h^2=0.025$ and 1 contours in the $m_{\tilde g}-\tan\beta$, $m_{\tilde\chi_1^\pm}-\tan\beta$, $m_{\tilde\chi_1^0}-\tan\beta$, and $m_{\tilde\chi_2^0}-\tan\beta$, parameter spaces. That is, we simply convert from $\delta_{\rm GS}$ to one of the indicated masses. These four sets of contours appear in Fig. 19. We observe that, for small to moderate $\tan\beta$ values, the upper bounds on the masses set by $\Omega h^2<1$ are such that the $\tilde\chi_1^\pm$ and $\tilde\chi_2^0$ should be observable at LEP-II (keeping in mind that the maximum masses occur for large $-\delta_{\rm GS}$ for which $\Delta m_{\tilde\chi_1}$ is big enough that direct $\tilde\chi_1^+\tilde\chi_1^-$ detection should be feasible) and such that $\tilde g\tilde g$ detection at the Tevatron should be possible. At larger $\tan\beta$ [$\gtrsim$5–10, depending upon sgn(μ)], the masses begin to exceed the reach of LEP-II and the Tevatron. Large masses for the gauginos are also possible if $-\delta_{\rm GS}$ is very small. However, as noted already, if we require $\Omega h^2>0.025$ then $-\delta_{\rm GS}$ can never be small (see Fig. 18). Together, the $\Omega h^2>0.025$ and $\Omega h^2<1$ bounds imply that the gaugino masses must all lie in mass regions that are eminently accessible at the NLC and LHC, and very possibly at LEP-II and the Tevatron.[7] With regard to the Higgsino-like chargino and neutralinos, we refer back to Fig. 9, where the $\Omega h^2=0.025$ and 1 contours were given. We observe that if $\tan\beta\gtrsim 4$–5 then Higgsino discovery at a $\sqrt{s}=500$ GeV e^+e^- collider will generally be possible for model parameters consistent with $0.025\lesssim\Omega h^2\lesssim 1$.

Finally, we note that the Ωh^2 contours are not sensitive to the m_0 value if $m_0\gtrsim 200$ GeV so that the coannihilation cross section is mainly determined by the s-channel W pole graph. Thus, even though m_0 could be substantially below 1 TeV for small $-\delta_{\rm GS}$ without violating $m_{\tilde\chi_1^\pm}\gtrsim 47$ GeV (due to the $m_0/\sqrt{-\delta_{\rm GS}}$ growth of the $|M_i^0|$'s) small $-\delta_{\rm GS}$ values would continue to be ruled out if $\Omega h^2\gtrsim 0.025$ is required.

[7]This is not dissimilar to the conclusion that is reached in the case of universal boundary conditions if m_0 is large. There, if m_0 is large enough ($\gtrsim$300 GeV) to suppress t-channel annihilation contributions to $\tilde\chi_1^0\tilde\chi_1^0$ annihilation, then the $\tilde\chi_1^0$ must be light enough that annihilation via a nearby s-channel Higgs and/or Z pole is sufficiently efficient. Typically [21], $m_{\tilde\chi_1^0}\lesssim 55$ GeV or so is required.

III. FINAL REMARKS AND CONCLUSIONS

The moduli dominated limit of string SUSY breaking yields a rich phenomenology that differs substantially from that obtained for the usual M_U-scale universal boundary conditions. In this paper we have considered a specific orbifold model (the O-II model) in which the moduli dominated limit can be taken and the M_U-scale boundary conditions computed. The model and its phenomenology are determined by $\tan\beta$ (the standard Higgs vacuum expectation value ratio), $\delta_{\rm GS}$ (the Green-Schwarz mixing parameter), and the universal scalar mass at M_U, m_0. Theoretically, negative integer values for $\delta_{\rm GS}$ in the range $|\delta_{\rm GS}|<5$–6 are preferred. For such values, the gaugino masses at M_U, which only arise at one-loop, are very non-universal; universality is approached, but *very* slowly, as $|\delta_{\rm GS}|$ becomes very large. Further, the (one-loop) M_U-scale gaugino masses, $|M_i^0|$, will be very much smaller than m_0. The nonuniversality of the gaugino masses at M_U implies that it is very possible that the lightest chargino and neutralino will both be SU(2) gauginos and, therefore, approximately degenerate, $m_{\widetilde{\chi}_1^\pm}\simeq m_{\widetilde{\chi}_1^0}$. Further, it is also possible for the gluino to be degenerate with both just outside the region $\delta_{\rm GS}\sim -3$ that is excluded by virtue of requiring $m_{\widetilde{g}}\gtrsim m_{\widetilde{\chi}_1^0}$, i.e. that the gluino not be the LSP. If $|\delta_{\rm GS}|$ is of moderate size, implying $m_0\gtrsim|M_i^0|$, the gauginos will be relatively light provided $m_0\lesssim 2$ TeV (as presumably required by naturalness); indeed, $m_0\gtrsim 1$ TeV if $m_{\widetilde{\chi}_1^\pm}\gtrsim m_Z/2$, as required by LEP data. When m_0 is large, squarks, sleptons, and heavy Higgs bosons will be very massive. Further, correct electroweak symmetry breaking implies that μ will be large. Thus, the most accessible SUSY signals will be those deriving from gaugino ($\widetilde{g}$, $\widetilde{\chi}_1^\pm$, $\widetilde{\chi}_1^0$, and $\widetilde{\chi}_2^0$) production.

The mass degeneracies noted above are of particular phenomenological importance. Key implications at existing and future accelerators include the following.

If $m_{\widetilde{\chi}_1^\pm}-m_{\widetilde{\chi}_1^0}$ is small (as for theoretically preferred model parameters) it will be necessary to employ $e^+e^-\to\gamma\widetilde{\chi}_1^+\widetilde{\chi}_1^-$ final states at LEP-II and the NLC for light chargino detection due to the near invisibility of the $\widetilde{\chi}_1^\pm$ decays.

The small size of $e^+e^-\to\widetilde{\chi}_1^0\widetilde{\chi}_2^0, \widetilde{\chi}_2^0\widetilde{\chi}_2^0$ cross sections (due to the state compositions predicted by the model) and the large masses of the $\widetilde{\chi}_2^\pm$, $\widetilde{\chi}_3^0$ and $\widetilde{\chi}_4^0$ (due to the large value of $|\mu|$ predicted), imply that only at the NLC can one hope for substantial numbers of neutralino and chargino pair events other than the difficult to detect $\widetilde{\chi}_1^+\widetilde{\chi}_1^-$ process.

If $m_{\widetilde{g}}\sim m_{\widetilde{\chi}_1^\pm}\simeq m_{\widetilde{\chi}_1^0}$ (as for theoretically preferred model parameters), $\widetilde{g}\widetilde{g}$ production will be more difficult to detect at both the Tevatron and the LHC due to the softness of the jets in $\widetilde{g}$ decay. Weak jet cuts must be employed, implying large background and difficulty in achieving adequate S/B.

If $m_{\widetilde{g}}$ is not nearly degenerate with $m_{\widetilde{\chi}_1^\pm}\simeq m_{\widetilde{\chi}_1^0}$, $\widetilde{g}\widetilde{g}$ discovery in the jets$+\not{E}_T$ channel (using weak jets cuts) at the Tevatron/TeV* could be easier than observation of neutralino and chargino pair production at a $\sqrt{s}=500$ GeV NLC.

Detection of $\widetilde{g}\widetilde{g}$ production at the LHC will require significant alterations in the cuts currently employed.

If $m_{\widetilde{\chi}_1^\pm}\simeq m_{\widetilde{\chi}_1^0}$, the degeneracy will be manifest at a hadron collider as an absence of like-sign dilepton signals for $\widetilde{g}\widetilde{g}$ production and of trilepton signals for $\widetilde{\chi}_1^\pm\widetilde{\chi}_2^0$ production.

In addition to accelerator implications listed above, there are two cosmology-related features of the model.

For the preferred $|\delta_{\rm GS}|\lesssim 5$–$6$ range, $\Omega h^2<0.025$ (the minimum required if the $\widetilde{\chi}_1^0$ is to be a significant dark matter candidate). Such small values of Ωh^2 are a result of the large $\widetilde{\chi}_1^\pm\widetilde{\chi}_1^0$ coannihilation rate when $m_{\widetilde{\chi}_1^\pm}\simeq m_{\widetilde{\chi}_1^0}$.

If $\delta_{\rm GS}$ is chosen as a function of $\tan\beta$ so that $0.025\lesssim\Omega h^2\lesssim 1$, then for moderate $\tan\beta$ the $\widetilde{g}$, $\widetilde{\chi}_1^\pm$, and $\widetilde{\chi}_2^0$ masses are relatively modest in size. In particular, they are such that proper analysis of existing Tevatron data and soon-to-come LEP-II data will exclude $\tan\beta\lesssim 5$–10.

ACKNOWLEDGMENTS

This work was supported in part by U.S. Department of Energy Grant Nos. DE-FG03-91ER40674 (J.F.G., C.H.C.) and DE-FG02-95ER40896 (M.D.), the Davis Institute for High Energy Physics, the Wisconsin Research Committee using funds granted by the Wisconsin Alumni Research Foundation (M.D.), and by a grant from the Deutsche Forschungsgemeinschaft under the Heisenberg program (M.D.).

APPENDIX A: CHARGINO DECAYS

In this appendix we discuss the calculation of the partial widths for leptonic and hadronic chargino decays for small mass splitting between the chargino and the lightest neutralino. We saw in Fig. 4 that even after inclusion of one-loop radiative corrections [7,8] this mass difference can be as small as 150 MeV. Standard expressions for $\widetilde{\chi}_1^\pm\to\widetilde{\chi}_1^0 f f'$ are not applicable for such small mass differences, since they assume the final-state fermions f and f' to be massless. Moreover, hadronic decays can only be described by perturbative QCD if the mass difference exceeds one or two GeV.

Allowing a finite mass for the standard model fermions produced in chargino decays is straightforward. First, we can ignore sfermion and charged Higgs exchange diagrams, since these particles are very heavy, and the $\widetilde{\chi}_1^\pm\widetilde{\chi}_1^0 W$ coupling is maximal in the relevant limit where both the chargino and the neutralino are almost pure SU(2) gauginos. Further, we actually only need to keep the mass of one of the two SM fermions; the other one is either much lighter (as for $f=c$, $f'=s$) or exactly massless (for $f=l$, $f'=\nu_l$). The result can be written as

$$\Gamma(\widetilde{\chi}_1^-\to\widetilde{\chi}_1^0 f\overline{f'})=\frac{N_c G_F^2}{(2\pi)^3}\left\{\widetilde{m}_-[(O_{11}^L)^2+(O_{11}^R)^2]\int_{(\widetilde{m}_0+m_f)^2}^{\widetilde{m}_-^2}dq^2\left(1-\frac{\widetilde{m}_0^2+m_f^2}{q^2}\right)\left(1-\frac{q^2}{\widetilde{m}_-^2}\right)^2\sqrt{\lambda(q^2,\widetilde{m}_0^2,m_f^2)}\right.$$
$$\left.-2\widetilde{m}_0 O_{11}^L O_{11}^R\int_{m_f^2}^{(\widetilde{m}_--\widetilde{m}_0)^2}dq^2\,\frac{q^2}{\widetilde{m}_-^2}\left(1-\frac{m_f^2}{q^2}\right)^2\sqrt{\lambda(\widetilde{m}_-^2,\widetilde{m}_0^2,q^2)}\right\}. \tag{A1}$$

Here, $\lambda(a,b,c)=(a+b-c)^2-4ab$ is the standard kinematical function, $N_c=3(1)$ if f is a quark (lepton), $O_{11}^{R,L}$ are the $\widetilde{\chi}_1^{\pm}\widetilde{\chi}_1^0 W$ couplings in the notation of Ref. [22], and we have introduced the shorthand notation $\widetilde{m}_0 \equiv m_{\widetilde{\chi}_1^0}$, $\widetilde{m}_- \equiv m_{\widetilde{\chi}_1^{\pm}}$. In the limit where both $\widetilde{\chi}_1^{\pm}$ and $\widetilde{\chi}_1^0$ are pure SU(2) gauginos, $O_{11}^L=O_{11}^R=1$.

As mentioned earlier, Eq. (A1) can only describe hadronic $\widetilde{\chi}_1^{\pm}$ decays if the chargino-neutralino mass difference $\Delta m_{\widetilde{\chi}}$ is sufficiently large. For $\Delta m_{\widetilde{\chi}}<1-2$ GeV one instead has to explicitly sum over exclusive hadronic final states. Fortunately much work on the related case of semileptonic τ decays has already been done. We adopt the formalism developed in Ref. [23].

As already stated in the main text, the partial width for the simplest hadronic decay, $\widetilde{\chi}_1^- \to \pi^- \widetilde{\chi}_1^0$, is tiny; it only proceeds through the axial vector coupling $\propto O_{11}^R - O_{11}^L$, which is very small for small $\Delta m_{\widetilde{\chi}}$. The partial width into final states with 3 pions is suppressed for the same reason. Partial widths into final states containing kaons are suppressed by a factor of $\sin^2\theta_c \simeq 1/20$. For our purposes it is therefore sufficient to only include the decay $\widetilde{\chi}_1^- \to \widetilde{\chi}_1^0 \pi^- \pi^0$. The partial width can be written as [23]

$$\Gamma(\widetilde{\chi}_1^- \to \widetilde{\chi}_1^0 \pi^- \pi^0) = \frac{G_F^2 (O_{11}^L + O_{11}^R)^2}{192\pi^3 \widetilde{m}_-^3} \int_{4m_\pi^2}^{(\Delta m_{\widetilde{\chi}})^2} dq^2 |F(q^2)|^2 \left(1 - \frac{4m_\pi^2}{q^2}\right) \left[\widetilde{m}_-^2 + \widetilde{m}_0^2 - 2q^2 + \frac{(\widetilde{m}_-^2 - \widetilde{m}_0^2)^2}{q^2} - 6\widetilde{m}_- \widetilde{m}_0\right] \times \sqrt{\lambda(\widetilde{m}_-^2, \widetilde{m}_0^2, q^2)}. \tag{A2}$$

The form factor $F(q^2)$ is dominated by the ρ and ρ' meson poles:

$$F(q^2) = \frac{P_{\mathrm{BW}_\rho}(q^2) + \beta P_{\mathrm{BW}_\rho}(q^2)}{1+\beta}. \tag{A3}$$

Here P_{BW} stands for a Breit-Wigner pole:

$$P_{\mathrm{BW}_V}(q^2) = \frac{m_V^2}{m_V^2 - q^2 - i\sqrt{q^2}\Gamma_V}, \tag{A4}$$

with $V=\rho,\rho'$. Following Ref. [23] we use $\beta=-0.145$ in Eq. (A3), and $m_\rho=773$ MeV, $\Gamma_\rho=145$ MeV, $m_{\rho'}=1370$ MeV, and $\Gamma_{\rho'}=510$ MeV in Eq. (A4). We use Eq. (A2) to describe hadronic $\widetilde{\chi}_1^{\pm}$ decays as long as it predicts a larger partial width than Eq. (A1) does; we use a constituent-type effective mass for the d quark of 500 MeV in our calculation (recall that we assume $m_u=0$; using a single large constituent mass to describe the kinematics should be sufficient for us). Figure 6 shows that this prescription implies a switchover from Eq. (A2) to Eq. (A1) at $\Delta m_{\widetilde{\chi}} \simeq 2$ GeV.

APPENDIX B: THE LSP RELIC DENSITY

Our calculation of the present mass density of LSP's left over from the Big Bang follows the treatment of Ref. [24]. The physical picture is that the LSP remains in thermal equilibrium until the Universe has cooled to the temperature T_F where the LSP ''freezes out.'' At lower temperatures essentially no further LSP's are produced, but occasionally two of them still annihilate into standard model particles, thereby reducing the relic density. In our case we have to deal with the additional complication [7] that the LSP might be almost degenerate in mass with the lightest chargino. In this case reactions that convert a neutralino into a chargino or vice versa, such as $\widetilde{\chi}_1^0 + f \leftrightarrow \widetilde{\chi}_1^{\pm} + f'$, remain in thermal equilibrium long after the LSP density itself has dropped out of equilibrium. The reason is that the rate for such conversion reactions is proportional to the product of the small LSP density and a large density of some SM fermion, whereas the rate for LSP annihilation processes is proportional to the *square* of the small LSP relic density. The chargino density is therefore simply given by the neutralino density times a Boltzmann factor. One can then include coannihilation effects by means of an effective LSP annihilation cross section.

Following Ref. [24], we first define the effective number of LSP degrees of freedom,

$$g_{\mathrm{eff}} = 2 + 4(1+\Delta_{\widetilde{\chi}})^{3/2} \exp(-\Delta_{\widetilde{\chi}} x), \tag{B1}$$

where we have introduced $\Delta_{\widetilde{\chi}} \equiv m_{\widetilde{\chi}_1^{\pm}}/m_{\widetilde{\chi}_1^0} - 1$ and the inverse rescaled temperature $x \equiv m_{\widetilde{\chi}_1^0}/T$. Notice that the LSP, being a Majorana fermion, only has two degrees of freedom, whereas the chargino has four. However, the contribution of the chargino is suppressed by the Boltzmann factor $\exp(-\Delta_{\widetilde{\chi}} x)$. The effective annihilation cross section is then given by

$$\sigma_{\mathrm{eff}} = \frac{4}{g_{\mathrm{eff}}^2}\, \sigma(\widetilde{\chi}_1^0 \widetilde{\chi}_1^0 \to \text{anything}) + \frac{16}{g_{\mathrm{eff}}^2}\, (1+\Delta_{\widetilde{\chi}})^{3/2} \times \exp(-\Delta_{\widetilde{\chi}} x)\, \sigma(\widetilde{\chi}_1^0 \widetilde{\chi}_1^- \to \text{anything}). \tag{B2}$$

Notice the relative factor of 4 between the first and the second term in Eq. (B2). One factor of 2 arises because of the larger number of chargino degrees of freedom, and another factor of 2 appears because here the initial state contains two different particles [24]. In principle we should also add terms for $\widetilde{\chi}_1^+ \widetilde{\chi}_1^-$ annihilation and, if $m_{\widetilde{\chi}_1^-} > m_W$, for $\widetilde{\chi}_1^- \widetilde{\chi}_1^-$ and $\widetilde{\chi}_1^+ \widetilde{\chi}_1^+$ annihilation. However, it turns out that the terms already included in Eq. (B2) are sufficient to reduce the relic density to a value that is too small to be of cosmological significance if the chargino-neutralino mass splitting is small, see Fig. 16; the exact value of the relic density is then of little interest. The relic density only reaches significant levels if the Boltzmann factor is already much smaller than 1. In this case the terms we have omitted are very small, since they are suppressed by the square of this factor.

Numerically, freeze-out occurs at $x=x_F\cong 20$. Since $x_F \gg 1$, the LSP's and charginos are quite nonrelativistic when they drop out of thermal equilibrium. Further, the low freeze-out temperature means that the coannihilation contribution to the effective cross section (B2) starts to become suppressed if the LSP-chargino mass difference exceeds a few percent. Nevertheless in our case the second term remains dominant out to quite large mass splittings, because the $\widetilde{\chi}_1^0\widetilde{\chi}_1^0$ annihilation term is strongly suppressed: since $\widetilde{\chi}_1^0$ is an almost pure gaugino state, its couplings to Z and Higgs bosons are small; further, sfermion exchange contributions are suppressed by the large sfermion masses required in this model, unless $|\delta_{\rm GS}|$ is either much smaller or much larger than 1. In contrast, the $\widetilde{\chi}_1^0\widetilde{\chi}_1^-$ annihilation cross section is quite large here, since the $\widetilde{\chi}_1^0\widetilde{\chi}_1^- W^+$ coupling is near its maximum in our case.

We computed the first term in Eq. (B2) including the full set of two-body final states treated in Ref. [25]. We used the usual nonrelativistic expansion of the cross sections in most cases, but treated the thermal average over Breit-Wigner factors due to s-channel exchange of Higgs and Z bosons more carefully [24], using a numerical method developed in Ref. [26]. In the second term of Eq. (B2) we only included ff' and $W\gamma$ final states, where f and f' are light SM fermions, whose masses we neglected. Since sfermions as well as the charged Higgs bosons are very heavy in the model we are studying, we only included contributions from the exchange of W bosons and (for the $W\gamma$ final state) the light chargino. As discussed in the main text, present experimental bounds imply that $m_{\widetilde{\chi}_1^-}+m_{\widetilde{\chi}_1^0}$ is well above m_W. We can therefore use the nonrelativistic expansion when calculating the coannihilation cross sections. The result is

$$\sigma(\widetilde{\chi}_1^0\widetilde{\chi}_1^-\to f\overline{f'})=\frac{N_c g^4}{64\pi}\frac{1}{(s-m_W^2)^2}\left\{s(O_{11}^R+\eta O_{11}^L)^2+v^2O_1^RO_{11}^L\widetilde{m}_0\widetilde{m}_-+\frac{v^2}{2}\left[(O_{11}^R)^2+(O_{11}^L)^2\right]\left[\frac{5}{3}\left|\widetilde{m}_0\right|\widetilde{m}_-+\widetilde{m}_-^2+\widetilde{m}_0^2\right]\right\}, \tag{B3}$$

$$\sigma(\widetilde{\chi}_1^0\widetilde{\chi}_1^-\to W^-\gamma)=\frac{\alpha_{\rm em}g^2}{8s}\left\{\left[(O_{11}^R)^2+(O_{11}^L)^2\right]\left[1+\left(\frac{\widetilde{m}_0}{\widetilde{m}_-}\right)^2\right](4+\gamma_W^2)-4\gamma_W^2O_{11}^LO_{11}^R\frac{\widetilde{m}_0}{\widetilde{m}_-}\right\}. \tag{B4}$$

Here, g is the SU(2) gauge coupling, N_c, $O_{11}^{R,L}$, $\widetilde{m}_0$ and $\widetilde{m}_-$ have been defined after Eq. (A1), v is the relative velocity between the chargino and the neutralino in their center-of-mass frame, and $s\equiv(|\widetilde{m}_0|+\widetilde{m}_-)^2$. Notice that, following Ref. [25], we are working in a convention where the neutralino mixing matrix is real; in that case we must allow the neutralino masses to have either sign, and η in Eq. (B3) is the sign of $\widetilde{m}_0$. The chargino masses can always be chosen to be positive even if we take the chargino mixing matrices to be real. Finally, $\gamma_W=E_W/m_W=(s+m_W^2)/(2m_W^2)$. The results of Eqs. (B3) and (B4) already include summing and averaging over spin and helicity states; the terms $\propto\gamma_W^2$ in Eq. (B4) are due to the production of longitudinal gauge bosons. Note that these terms cancel in the limit $\widetilde{m}_0=\widetilde{m}_-$, $O_{11}^L=O_{11}^R$; this ensures that the cross section drops like $1/s$ in the limit of large SU(2) gaugino mass M_2, as required by unitarity. Finally, since the contribution from Eq. (B4) turns out to be at least a factor of 10 smaller than that from Eq. (B3), we have only computed the leading $\mathcal{O}(v^0)$ term here.

[1] A. Lleyda and C. Munoz, Phys. Lett. B **317**, 82 (1993); D. Choudhury, F. Eberlein, A. Konig, J. Louis, and S. Pokorski, *ibid.* **342**, 180 (1995); M. Olechowski and S. Pokorski, *ibid.* **344**, 201 (1995); N. Polonsky and A. Pomarol, Phys. Rev. D **51**, 6532 (1995); D. Matalliotakis and H. P. Nilles, Nucl. Phys. **B435**, 115 (1995); P. Brax, U. Ellwanger, and C. A. Savoy, Phys. Lett. B **347**, 269 (1995); S. Dimopoulos and G. F. Giudice, *ibid.* **357**, 573 (1995); T. Kobayashi *et al.*, *ibid.* **348**, 402 (1995); R. Altendorfer and T. Kobayashi, Int. J. Mod. Phys. A **11**, 903 (1996).

[2] A. Brignole, L. E. Ibanez, and C. Munoz, Nucl. Phys. **B422**, 125 (1994); **B436**, 747(E) (1995).

[3] A. Brignole, L. E. Ibanez, C. Munoz, and C. Scheich, Report No. FTUAM-95-26, hep-ph/9508258 (unpublished).

[4] J. A. Casas, A. Lleyda, and C. Munoz, Phys. Lett. B **380**, 59 (1996).

[5] G. F. Giudice and A. Masiero, Phys. Lett. B **206**, 480 (1988).

[6] J. F. Gunion, H. E. Haber, G. L. Kane, and S. Dawson, *The Higgs Hunters Guide* (Addison-Wesley, Reading, MA, 1990).

[7] S. Mizuta, D. Ng, and M. Yamaguchi, Phys. Lett. B **300**, 96 (1993).

[8] A. Papadopoulos and D. Pierce, Nucl. Phys. **B430**, 278 (1994).

[9] L3 Collaboration, M. Acciarri *et al.*, Phys. Lett. B **377**, 289 (1996).

[10] C.-H. Chen, M. Drees, and J. F. Gunion, Phys. Rev. Lett. **76**, 2002 (1996).

[11] A. Bartl, H. Fraas, and W. Majerotto, Z. Phys. C **30**, 441 (1986); Nucl. Phys. **B278**, 1 (1986).

[12] T. Barklow (private communication).

[13] D0 Collaboration, S. Abachi *et al.*, Phys. Rev. Lett. **75**, 618 (1995).

[14] CDF Collaboration, J. Hauser, *Proceedings of the 10th Topical Workshop on Proton-Antiproton Collider Physics* (AIP, New York, 1995).

[15] H. Baer, C.-H. Chen, F. Paige, and X. Tata, Phys. Rev. D **54**, 5866 (1996).

[16] H. Baer, C.-H. Chen, F. Paige, and X. Tata, Phys. Rev. D **52**, 2746 (1995).
[17] T. Kamon, Institution Report No. CDF/PUB/EXOTIC/PUBLIC/3667, 1996 (unpublished).
[18] ATLAS Report No. CERN/LHCC/94-43, LHCC/P2, 1994 (unpublished).
[19] CMS Report No. CERN/LHCC 94-38, LHCC/P1, 1994 (unpublished).
[20] J. Womersley (private communication).
[21] P. Nath and R. Arnowitt, Phys. Rev. Lett. **70**, 3696 (1993); Phys. Lett. B **299**, 58 (1993); **307**, 403(E) (1993); J. L. Lopez, D. V. Nanopoulos, Ka-jia Yuan, Phys. Rev. D **48**, 2766 (1993); R. Arnowitt and P. Nath, *ibid.* **54**, 2374 (1996); in *From Superstring to Present Physics*, Proceedings of the International School of Subnuclear Physics, Erice, Italy, 1994 edited by A. Zrchichi (World Scientific, Singapore, 1995), Report No. hep-ph/9411350 (unpublished).
[22] H. E. Haber and G. L. Kane, Phys. Rep. **117**, 75 (1985).
[23] H. Kühn and A. Santamaria, Z. Phys. C **48**, 445 (1990).
[24] K. Griest and D. Seckel, Phys. Rev. D **43**, 3191 (1991).
[25] M. Drees and M. M. Nojiri, Phys. Rev. D **47**, 376 (1993).
[26] M. Drees and A. Yamada, Phys. Rev. D **53**, 1586 (1996).